JEM Journal of Experimental Medicine

ARTICLE

Innate immune priming in the absence of TAK1 drives RIPK1 kinase activity–independent pyroptosis, apoptosis, necroptosis, and inflammatory disease

R.K. Subbarao Malireddi[1*], Prajwal Gurung[1,2*], Sannula Kesavardhana[1], Parimal Samir[1], Amanda Burton[1], Harisankeerth Mummareddy[1], Peter Vogel[3], Stephane Pelletier[1], Sandeepta Burgula[4], and Thirumala-Devi Kanneganti[1]

RIPK1 kinase activity has been shown to be essential to driving pyroptosis, apoptosis, and necroptosis. However, here we show a kinase activity–independent role for RIPK1 in these processes using a model of TLR priming in a TAK1-deficient setting to mimic pathogen-induced priming and inhibition. TLR priming of TAK1-deficient macrophages triggered inflammasome activation, including the activation of caspase-8 and gasdermin D, and the recruitment of NLRP3 and ASC into a novel RIPK1 kinase activity–independent cell death complex to drive pyroptosis and apoptosis. Furthermore, we found fully functional RIPK1 kinase activity–independent necroptosis driven by the RIPK3–MLKL pathway in TAK1-deficient macrophages. In vivo, TAK1 inactivation resulted in RIPK3–caspase-8 signaling axis–driven myeloid proliferation and a severe sepsis-like syndrome. Overall, our study highlights a previously unknown mechanism for RIPK1 kinase activity–independent inflammasome activation and pyroptosis, apoptosis, and necroptosis (PANoptosis) that could be targeted for treatment of TAK1-associated myeloid proliferation and sepsis.

Introduction

Inflammasomes are multimeric protein complexes consisting of a cytoplasmic sensor, an apoptosis-associated speck-like protein containing a caspase-recruitment domain (ASC) adaptor, and the cysteine protease caspase-1 (Man and Kanneganti, 2016; Poudel and Gurung, 2018). Assembly of an inflammasome complex activates caspase-1, which has two major cellular consequences: production of the proinflammatory bioactive cytokines IL-1β and IL-18 and cell death induced by the pore-forming N-terminal fragment of gasdermin D (Kayagaki et al., 2015; Shi et al., 2015). The NLRP3 inflammasome is one of the most studied inflammasomes; it is activated in response to a wide array of pathogen-associated molecular patterns (PAMPs) and damage-associated molecular patterns. Conventional activation of the NLRP3 inflammasome requires two signals: a priming signal often provided through TLRs and an activation signal provided by molecules such as ATP, nigericin, alum, silica, or pore-forming toxins (Karki and Kanneganti, 2019). Although inflammasome activation is critical for protection against infection, this system comes with the cost of a potential predisposition to unwanted inflammatory diseases through excessive inflammasome activation. In line with this possibility, we recently reported the existence of a transforming growth factor-β (TGF-β)–activated kinase 1 (TAK1)–mediated mechanism of NLRP3 inflammasome quiescence under steady-state conditions; therefore, TAK1 deficiency provokes spontaneous NLRP3 activation and cell death in macrophages in the absence of any external stimulation (Malireddi et al., 2018).

TAK1 regulates cellular homeostasis and proinflammatory signaling to activate NF-κB and MAPKs downstream of several well-known receptors, including the TLRs, IL-1 receptor, and TNF receptor (Landström, 2010). In the TNF receptor–induced signaling cascade, receptor-interacting protein kinase 1 (RIPK1) and TAK1 are present in the same complex with TNF receptor type 1–associated death domain protein (also known as complex-I), which initiates NF-κB and ERK signaling (Ea et al., 2006). TAK1 is tightly regulated in cells, as both TAK1 inactivation (or deficiency) and TAK1 hyperactivation (or overexpression) promote cell death and inflammation (Guo et al., 2016; Mihaly et al., 2014). How the presence or absence of TAK1 regulates RIPK1 function and subsequent cell death has been an area of intense

[1]Department of Immunology, St. Jude Children's Research Hospital, Memphis, TN; [2]Inflammation Program, Infectious Diseases Division, Department of Internal Medicine, University of Iowa, Iowa City, IA; [3]Department of Pathology, St. Jude Children's Research Hospital, Memphis, TN; [4]Department of Microbiology, Osmania University, Hyderabad, Telangana, India.

*R.K.S. Malireddi and P. Gurung contributed equally to this paper; Correspondence to Thirumala-Devi Kanneganti: thirumala-devi.kanneganti@stjude.org.

debate, and the detailed cellular and molecular pathways involved remain incompletely understood. Here we show that TLR priming by PAMPs bypasses the requirement for RIPK1 kinase activity in promoting cell death and NLRP3 inflammasome activation during the physiologically relevant condition of TAK1 deficiency in myeloid cells. Furthermore, TLR priming results in recruitment of RIPK1 to the caspase-8 and FADD complex in TAK1-deficient macrophages. These data highlight the formation of a novel RIPK1 kinase activity–independent ripoptosome-like complex with caspase-8 and FADD that promotes cell death and NLRP3 inflammasome activation, driving neutrophilia and severe sepsis-like shock in mice.

Results

RIPK1 kinase activity–independent cell death occurs in TAK1-deficient macrophages

We recently highlighted the role of TAK1 in regulating cellular homeostasis (Malireddi et al., 2018). In contrast to its known role in promoting NF-κB and ERK activation (Landström, 2010), TAK1 restricts the tonic activation of NF-κB and ERK and the production of TNF under steady-state conditions (Malireddi et al., 2018). This homeostatic control mechanism prevents spontaneous RIPK1 kinase–driven activation of the NLRP3 inflammasome and cell death (Malireddi et al., 2018). Because microbes are ubiquitous and have evolved to inhibit host TAK1 signaling (Human Microbiome Project Consortium, 2012; Meinzer et al., 2012; Orth et al., 1999; Peterson et al., 2017), we investigated the cellular and molecular consequences of microbial (or TLR) priming on the role of RIPK1 under the conditions of TAK1 inactivation. TAK1 deficiency in bone marrow–derived macrophages (*Lyz2*$^{cre+}$ × *Tak1*$^{f/f}$ BMDMs) induces spontaneous cell death that depends on RIPK1 kinase activity (Malireddi et al., 2018). *Lyz2*$^{cre+}$ × *Tak1*$^{f/f}$ BMDMs underwent spontaneous cell death, as observed by SYTOX Green dye uptake after 2 and 6 h of culture (Fig. 1, A and B). Consistent with previous findings (Malireddi et al., 2018), the cell death observed in *Lyz2*$^{cre+}$ × *Tak1*$^{f/f}$ BMDMs was rescued in BMDMs isolated from a newly generated RIPK1 kinase-dead (*Ripk1*$^{KD/KD}$) mouse strain (Fig. 1, A and B; and Fig. S1, A and B). This result extends previous findings that RIPK1 kinase activity is crucial for inducing cell death in response to a wide variety of stimuli (Weinlich and Green, 2014) and demonstrates the important role of RIPK1 kinase activity in the induction of spontaneous cell death.

It has been shown that RIPK1 kinase activity is necessary for cell death and inflammasome activation induced by *Yersinia* infection and TAK1 inhibition (Malireddi et al., 2018; Orning et al., 2018; Sarhan et al., 2018). However, LPS priming of *Lyz2*$^{cre+}$ × *Tak1*$^{f/f}$ BMDMs promoted the induction of cell death independent of RIPK1 kinase activity (Fig. 1, C and D). Similarly, *Yersinia enterocolitica* infection of *Lyz2*$^{cre+}$ × *Tak1*$^{f/f}$ BMDMs induced cell death independent of RIPK1 kinase activity (Fig. 1, A and B; and Fig. S2, A and B). To examine whether the RIPK1 kinase activity–independent cell death in *Lyz2*$^{cre+}$ × *Tak1*$^{f/f}$ mice was specific to LPS/TLR4 stimulation, we stimulated *Lyz2*$^{cre+}$ × *Tak1*$^{f/f}$ × *Ripk1*$^{KD/KD}$ BMDMs with the TLR2 agonist Pam3CSK4 and the TLR3 agonist poly(I:C) (polyinosinic:polycytidylic acid). Cell death was observed in *Lyz2*$^{cre+}$ × *Tak1*$^{f/f}$ × *Ripk1*$^{KD/KD}$ BMDMs in response to both TLR ligands tested (i.e., TLR2 and TLR3 ligands; Fig. 1, A, B, E, and F; and Fig. S2 A). Consistent with previous findings (Malireddi et al., 2018), the spontaneous cell death was not rescued in *Lyz2*$^{cre+}$ × *Tak1*$^{f/f}$ × *Nlrp3*$^{-/-}$ BMDMs; however, the TLR priming enhanced the progression of cell death (Fig. 1, A–F). Thus, TLR priming through either MyD88- or TIR-domain-containing adapter-inducing IFN-β (TRIF)–signaling pathways bypasses the need for RIPK1 kinase activity to induce cell death in TAK1-deficient macrophages.

TLR priming induces NLRP3-dependent, but RIPK1 kinase activity–independent, inflammasome activation in TAK1-deficient cells

TAK1 deficiency induces spontaneous inflammasome activation that is promoted by RIPK1 kinase activity (Malireddi et al., 2018). Thus, we examined the consequences of TLR stimulation on inflammasome activation, using caspase-1 activation as the readout, in *Lyz2*$^{cre+}$ × *Tak1*$^{f/f}$ BMDMs that lacked RIPK1 kinase activity. As demonstrated previously, we observed spontaneous activation of caspase-1 (as evidenced by caspase-1 p20 bands) in *Lyz2*$^{cre+}$ × *Tak1*$^{f/f}$ BMDMs that depended on RIPK1 kinase activity (Fig. 2 A). TLR stimulation with LPS, PAM3CSK4, or poly(I:C) or *Y. enterocolitica* infection resulted in robust caspase-1 cleavage in *Lyz2*$^{cre+}$ × *Tak1*$^{f/f}$ BMDMs that was independent of RIPK1 kinase activity (Fig. 2 B and Fig. S2, C–E). TLR4 stimulation also induced proteolytic processing of caspase-3, caspase-8, and gasdermin D in *Lyz2*$^{cre+}$ × *Tak1*$^{f/f}$ × *Ripk1*$^{KD/KD}$ BMDMs, suggesting RIPK1 kinase activity–independent activation of apoptotic and pyroptotic pathways in TAK1-deficient cells (Fig. 2, A and B). The NLRP3 inflammasome is responsible for RIPK1 kinase activity–dependent caspase-1 activation in TAK1-deficient macrophages (Malireddi et al., 2018). To determine whether TLR-induced caspase-1 cleavage was also NLRP3 inflammasome-dependent, we stimulated *Lyz2*$^{cre+}$ × *Tak1*$^{f/f}$ × *Nlrp3*$^{-/-}$ BMDMs with LPS, Pam3CSK4, or poly(I:C). Although the TLR stimulation of *Lyz2*$^{cre+}$ × *Tak1*$^{f/f}$ × *Nlrp3*$^{-/-}$ BMDMs enhanced the progression of cell death (Fig. 1, A–F), caspase-1 activation was still not detected in these cells (Fig. 2, C–F). These results demonstrate that the requirement of NLRP3 for inflammasome activation is not affected by TLR priming and that TAK1-deficient BMDMs can undergo cell death independent of inflammasome activation. Together, these data also demonstrate that TLR priming alleviates the requirement of RIPK1 kinase activity to activate the inflammasome and cell death in TAK1-deficient macrophages.

Kinase-dead RIPK1 is essential for TAK1 deficiency–driven cell death and inflammasome activation

Since TLR priming bypassed the need for RIPK1 kinase activity in promoting inflammasome activation and cell death in TAK1-deficient BMDMs, we next examined whether RIPK1 is totally dispensable under similar conditions, using RIPK1-deficient cells. To this end, we generated WT and *Ripk1*$^{-/-}$ macrophages from fetal liver cells (*Ripk1*$^{-/-}$ mice are perinatally lethal; Kelliher et al., 1998). TAK1 inhibitor (TAK1-i) treatment of

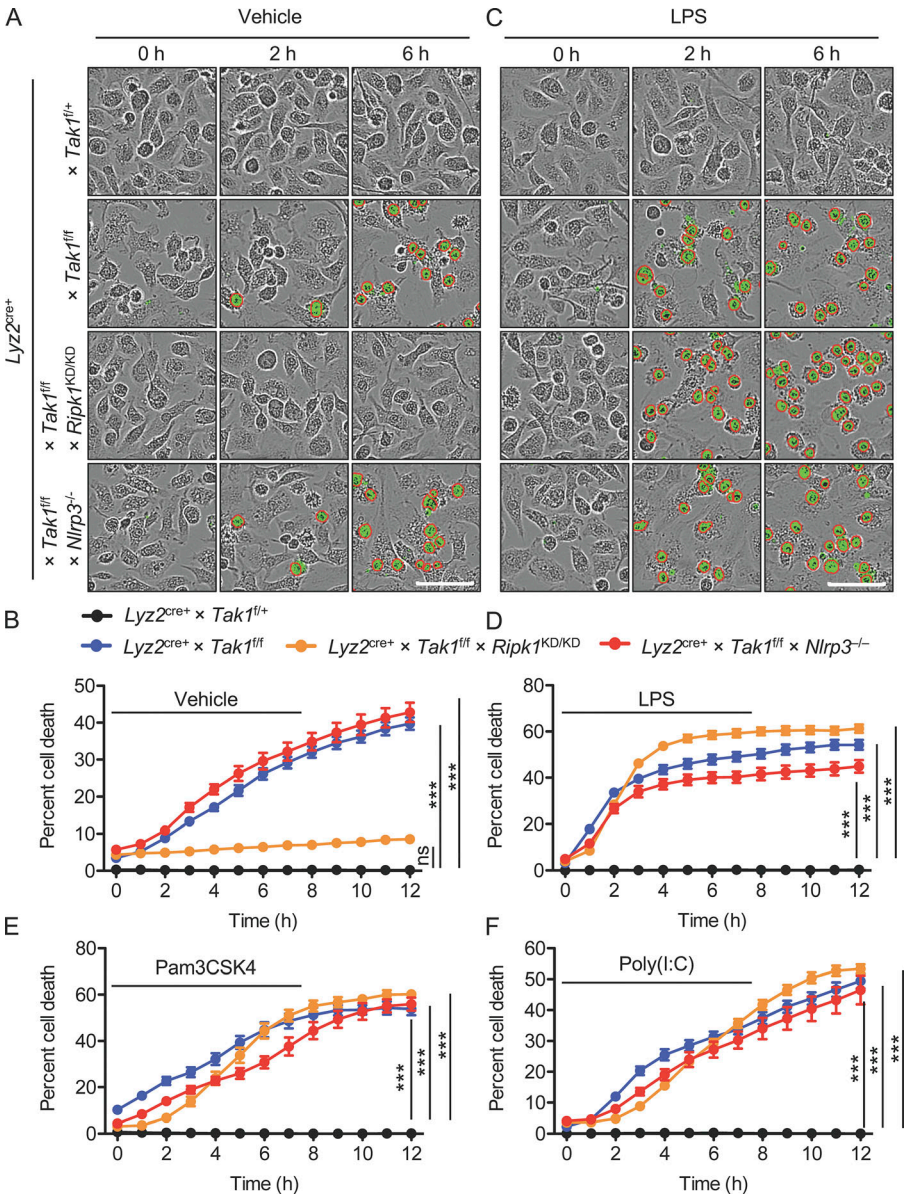

Figure 1. **TLR priming–induced cell death in TAK1-deficient macrophages does not depend on RIPK1 kinase activity. (A and B)** Cell death analysis of BMDMs from *Lyz2*$^{cre+}$ × *Tak1*$^{f/+}$ mice compared with BMDMs from *Lyz2*$^{cre+}$ × *Tak1*$^{f/f}$, *Lyz2*$^{cre+}$ × *Tak1*$^{f/f}$ × *Ripk1*$^{KD/KD}$, and *Lyz2*$^{cre+}$ × *Tak1*$^{f/f}$ × *Nlrp3*$^{-/-}$ mice. Cell death detected by IncuCyte image (A) and time-course analysis (B) of BMDMs treated with vehicle control assessed in culture at the indicated time points. Green with red circles indicates dead-cell positivity for SYTOX Green stain. Scale bars, 100 µm. **(C and D)** Cell death detected by IncuCyte image (C) and time-course analysis (D) of BMDMs treated with LPS. **(E and F)** Time-course analysis of cell death in BMDMs treated with Pam3CSK4 (E) or poly(I:C) (F). P values < 0.05 were considered statistically significant. ns, not significant. ***, P < 0.001 (one-way ANOVA with Dunnett's multiple comparisons test; B and D–F). Data are presented as mean ± SEM (B and D–F) and are representative of five independent experiments with similar results with three technical replicates per sample (A–F).

macrophages for 12 h induced inflammasome activation, as demonstrated by caspase-1 cleavage in WT but not *Ripk1*$^{-/-}$ macrophages (Fig. 3 A). Moreover, LPS or TNF stimulation of TAK1-i-treated *Ripk1*$^{-/-}$ macrophages failed to activate caspase-8 and the NLRP3 inflammasome, suggesting the requirement of full-length RIPK1 (RIPK1-scaffold function; Fig. 3 B). In concurrence with the lack of caspase-1 and caspase-8 activation, *Ripk1*$^{-/-}$ macrophages were resistant to cell death induced by TAK1 inactivation, both in the presence and in the absence of TNF or LPS priming (Fig. 3, C and D). However, consistent with our genetic data, we also observed that pharmacological inhibition of TAK1 followed by LPS priming induced cell death and inflammasome activation in RIPK1 kinase-dead (*Ripk1*$^{KD/KD}$) BMDMs (Fig. 3, E and F). Together, these observations suggest that TAK1 deficiency, when combined with TLR priming, promotes RIPK1-dependent (scaffold) but kinase activity–independent cell death and NLRP3 inflammasome activation.

TLR priming promotes the formation of RIPK1 kinase activity–independent multiprotein cell death complex in TAK1-deficient cells

In TAK1-deficient BMDMs, RIPK1 kinase activity promoted spontaneous NLRP3 inflammasome activation in the absence of external stimuli, but upon LPS priming, RIPK1 kinase activity–independent function promoted NLRP3 inflammasome activation and cell death. To investigate the role of RIPK1 recruitment into the cell death complex, we used fluorescence microscopy of *Lyz2*$^{cre+}$ × *Tak1*$^{f/+}$ (control) and *Lyz2*$^{cre+}$ × *Tak1*$^{f/f}$ × *Ripk1*$^{KD/KD}$ (TAK1-deficient and RIPK1 kinase-dead) BMDMs after LPS stimulation and probed for the presence of RIPK1, ASC, and caspase-8. RIPK1 colocalized with ASC and caspase-8 in a single punctum in LPS-primed *Lyz2*$^{cre+}$ × *Tak1*$^{f/f}$ × *Ripk1*$^{KD/KD}$ BMDMs but not in unprimed cells, suggesting that the RIPK1 complex formed independently of RIPK1 kinase activity (Fig. 4 A). Coimmunoprecipitation studies showed that in the absence of external stimuli, RIPK1 did not pull down NLRP3 or ASC in

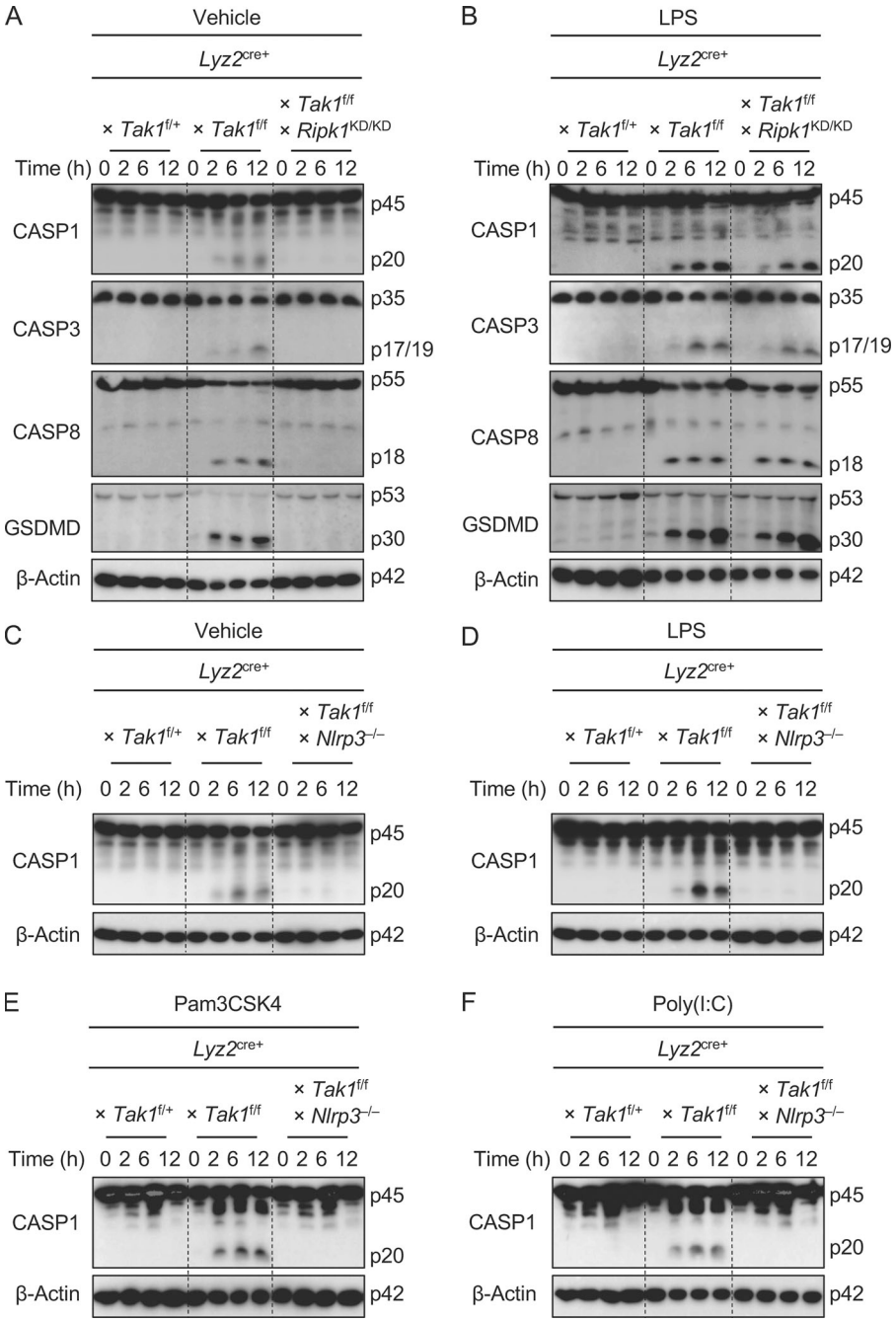

Figure 2. **TLR priming bypasses the requirement for RIPK1 kinase activity, but not NLRP3, to drive caspase-1 activation in TAK1-deficient macrophages. (A and B)** Western blot analyses of the activated caspase-1 subunit p20, activated caspase-3 subunit p17/19, activated caspase-8 subunit p18, and gasdermin D (GSDMD) subunit p30 from the lysates of *Lyz2*$^{cre+}$ × *Tak1*$^{f/+}$, *Lyz2*$^{cre+}$ × *Tak1*$^{f/f}$, or *Lyz2*$^{cre+}$ × *Tak1*$^{f/f}$ × *Ripk1*$^{KD/KD}$ BMDMs treated with vehicle control (A) or LPS (B) for the indicated times in culture after stimulation. **(C–F)** Western blot analysis of the active caspase-1 subunit p20 from the lysates of *Lyz2*$^{cre+}$ × *Tak1*$^{f/+}$, *Lyz2*$^{cre+}$ × *Tak1*$^{f/f}$, and *Lyz2*$^{cre+}$ × *Tak1*$^{f/f}$ × *Nlrp3*$^{-/-}$ BMDMs treated with vehicle control (C), LPS (D), Pam3CSK4 (E), or poly(I:C) (F). The "p" in Western blots denotes protein molecular weights. Data are representative of five independent experiments with similar results, with two technical replicates per sample (A–F).

control BMDMs but pulled down both in *Lyz2*$^{cre+}$ × *Tak1*$^{f/f}$ BMDMs, suggesting a spontaneous interaction between RIPK1 and the NLRP3 inflammasome in TAK1-deficient macrophages (Fig. 4 B, left panel). Furthermore, this spontaneous RIPK1 interaction with NLRP3 and ASC was abrogated in *Lyz2*$^{cre+}$ × *Tak1*$^{f/f}$ × *Ripk1*$^{KD/KD}$ BMDMs, suggesting that RIPK1 kinase activity drove spontaneous NLRP3 inflammasome assembly in unprimed TAK1-deficient BMDMs (Fig. 4 B, left panel). After LPS priming, the association of RIPK1 with NLRP3 and ASC was observed in *Lyz2*$^{cre+}$ × *Tak1*$^{f/f}$ BMDMs; however, this interaction was also observed in *Lyz2*$^{cre+}$ × *Tak1*$^{f/f}$ × *Ripk1*$^{KD/KD}$ BMDMs (Fig. 4 B, right panel). Together, these studies demonstrate that TLR priming of *Tak1*$^{f/f}$ × *Lyz2*$^{cre+}$ BMDMs switches the kinase-dependent association of RIPK1 with NLRP3 and ASC to a kinase activity–independent process of assembling a noncanonical ripoptosome-like cell death complex.

In TAK1-deficient macrophages, we observed that RIPK1 was recruited to the caspase-8–containing cell death complex (Fig. 4 A). Moreover, RIPK1 is a potent upstream activator of the RIPK3–caspase-8–mediated cell death pathway (Weinlich and Green, 2014). We therefore sought to address the effect of priming on the role of the RIPK3–caspase-8 axis in cell death and inflammasome activation in TAK1-deficient cells. Caspase-8 and FADD deficiency are embryonically lethal in mice, but the addition of RIPK3 deficiency rescues this embryonic lethality (Dillon et al., 2012; Kaiser et al., 2011; Oberst et al., 2011; Zhang

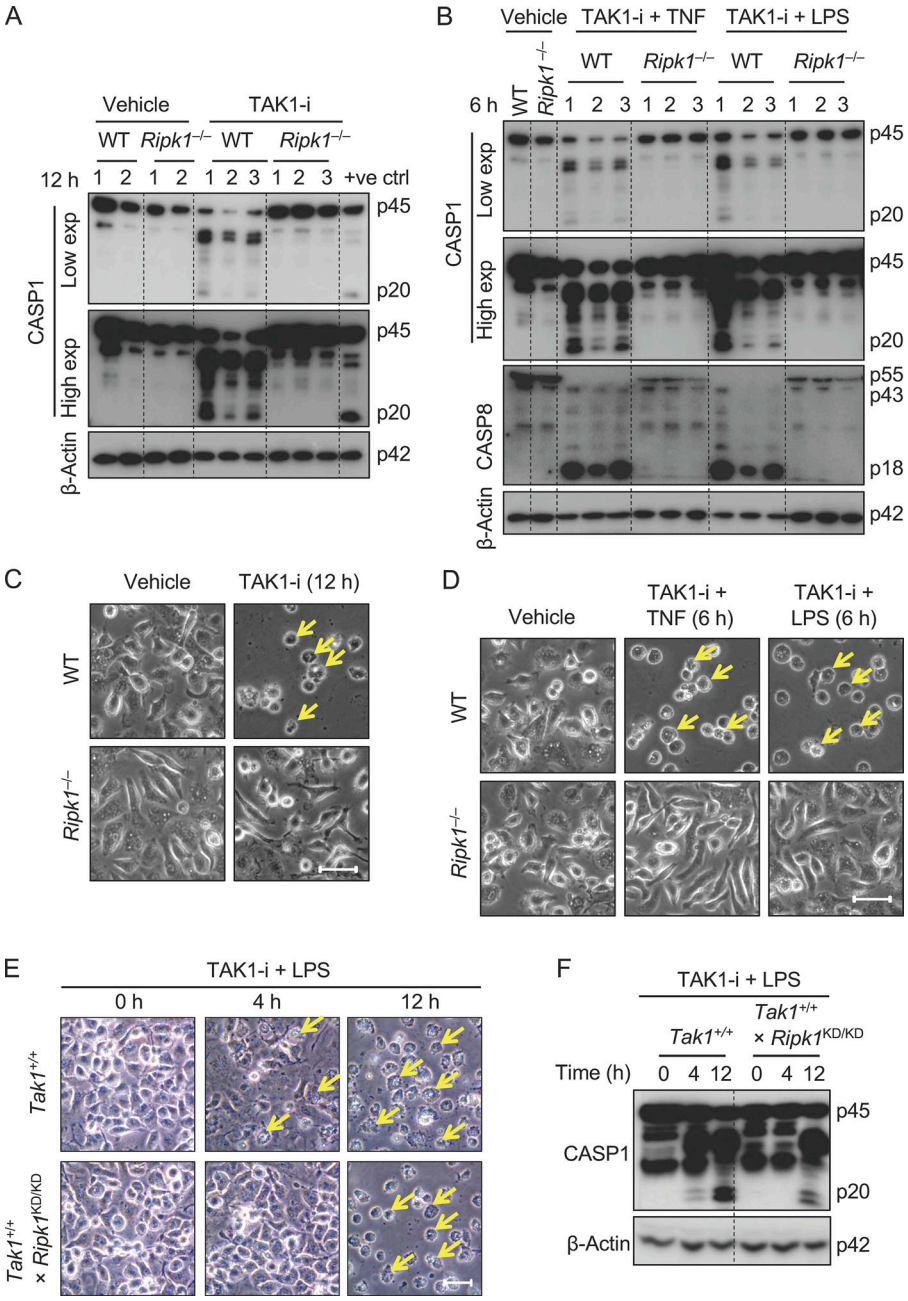

Figure 3. **TLR priming switches cell death and inflammasome activation in TAK1-deficient BMDMs to a RIPK1 scaffold–dependent process. (A)** Western blot analysis of the activated caspase-1 subunit p20 measured at 12 h after stimulation from the vehicle- or TAK1-i–treated WT and *Ripk1*$^{-/-}$ fetal liver–derived macrophages in the absence of priming and from the TAK1-i–treated BMDMs as a positive control (+ve ctrl BMDMs). **(B)** Western blot analysis of the activated caspase-1 subunit p20 and caspase-8 subunit p18 measured at 6 h after stimulation from the vehicle- or TAK1-i–treated WT and *Ripk1*$^{-/-}$ fetal liver macrophages in the presence of TNF or LPS stimulation. **(C and D)** Microscopic analysis of cell death in vehicle- or TAK1-i–treated cells (C) or in vehicle- or TNF + TAK1-i– or LPS + TAK1-i–treated cells (D). **(E and F)** Cell death detected by microscopic image analysis (E) or Western blot analysis of the active caspase-1 subunit p20 (F) from BMDMs treated with TAK1-i and LPS at the indicated times. BMDMs were obtained from *Tak1*$^{+/+}$ and kinase-dead RIPK1 (*Tak1*$^{+/+}$ × *Ripk1*$^{KD/KD}$) mice. Yellow arrows indicate dead cells. Scale bars, 50 µm (C–E). The "p" in Western blots denotes protein molecular weight. Data are representative of two (A–D) or three (E and F) independent experiments with at least two biological replicates and two (E and F) or three technical replicates per sample (A–D).

et al., 2011). Therefore, to study caspase-8 functions, we used BMDMs from *Ripk3*$^{-/-}$ mice as controls and compared their responses with those of *Ripk3*$^{-/-}$ × *Casp8*$^{-/-}$ and *Ripk3*$^{-/-}$ × *Fadd*$^{-/-}$ BMDMs following TAK1-i treatment in the presence or absence of TLR priming. Consistent with earlier studies (Orning et al., 2018; Sarhan et al., 2018), stimulation by TAK1-i or LPS + TAK1-i induced caspase-1 cleavage and cell death in *Ripk3*$^{-/-}$ BMDMs but not in *Ripk3*$^{-/-}$ × *Casp8*$^{-/-}$ or *Ripk3*$^{-/-}$ × *Fadd*$^{-/-}$ BMDMs (Fig. S3, A–C). In addition, Pam3CSK4 and poly(I:C) also failed to induce cell death and caspase-1 activation in TAK1-i–treated *Ripk3*$^{-/-}$ × *Casp8*$^{-/-}$ and *Ripk3*$^{-/-}$ × *Fadd*$^{-/-}$ macrophages (Fig. S3, D–F). Moreover, we also confirmed the specificity of these findings by genetic deletion of TAK1, RIPK3, and caspase-8 using BMDMs prepared from *Lyz2*$^{cre+}$ × *Tak1*$^{f/f}$ × *Ripk3*$^{-/-}$ × *Casp8*$^{-/-}$ mice (Fig. S4, A and B). Thus, under the conditions of TAK1 deficiency, TLR priming through either the TLR adapter MyD88 (Pam3CSK4) or TRIF (poly(I:C)) is sufficient to promote assembly of a RIPK1 kinase activity–independent cell death complex with FADD and caspase-8, which can drive potent inflammatory cell death and inflammasome activation.

Priming switches on RIPK1 kinase activity–independent activation of mixed-lineage kinase domain–like pseudokinase (MLKL) and necroptosis induction in TAK1-deficient cells

Given that TLR stimulation–induced cell death in *Lyz2*$^{cre+}$ × *Tak1*$^{f/f}$ BMDMs was independent of RIPK1 kinase activity, we next investigated the requirement of RIPK1 kinase activity for promoting necroptosis. As expected, LPS + z-VAD (a prototypical

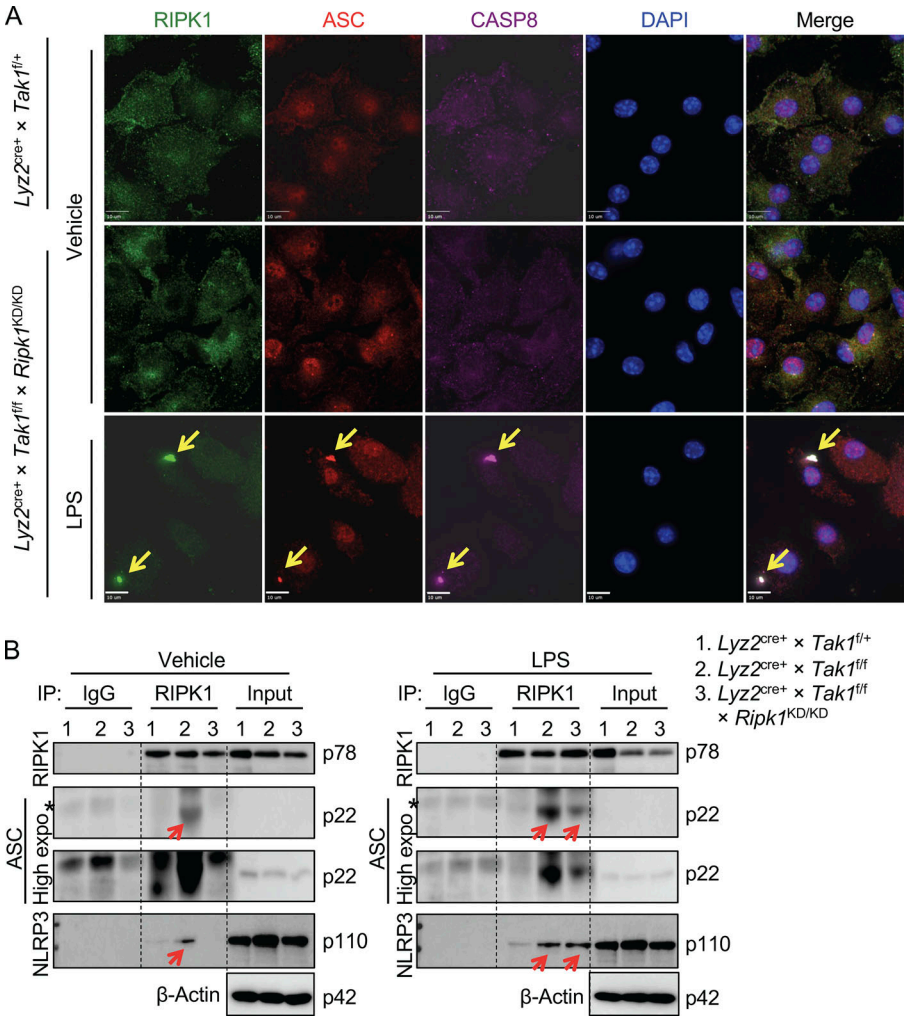

Figure 4. **TLR priming bypasses the requirement for RIPK1 kinase activity to assemble the multiprotein cell death complex in TAK1-deficient cells. (A)** Immunofluorescence staining and confocal microscopic analyses of RIPK1 (green), ASC (red), and caspase-8 (magenta) in unprimed BMDMs or those primed with LPS for 2 h. Nuclei were stained with DAPI (blue). BMDMs were obtained from *Lyz2*$^{cre+}$ × *Tak1*$^{f/+}$ or *Lyz2*$^{cre+}$ × *Tak1*$^{f/f}$ × *Ripk1*$^{KD/KD}$ mouse strains. Yellow arrows indicate the cell death complex. Scale bars, 10 µm. **(B)** Immunoprecipitation (IP) of endogenous RIPK1 from lysates of *Lyz2*$^{cre+}$ × *Tak1*$^{f/+}$ (1), *Lyz2*$^{cre+}$ × *Tak1*$^{f/f}$ (2), and *Lyz2*$^{cre+}$ × *Tak1*$^{f/f}$ × *Ripk1*$^{KD/KD}$ (3) BMDMs treated with vehicle control or LPS for 2 h and immunoblotted for RIPK1, ASC, and NLRP3 (n = 3). Red arrows indicate immunoprecipitated ASC and NLRP3, and black asterisks indicate nonspecific signal. The "p" in Western blots denotes protein molecular weight. Data are representative of three (A) or two (B) independent experiments with two technical replicates per sample.

necroptotic stimulus) promoted necroptosis in *Lyz2*$^{cre+}$ × *Tak1*$^{f/+}$ (control) BMDMs, and this cell death was abrogated in kinase-dead RIPK1 (*Lyz2*$^{cre+}$ × *Tak1*$^{f/+}$ × *Ripk1*$^{KD/KD}$) BMDMs or cells deficient in TAK1, RIPK3, and caspase-8 (*Lyz2*$^{cre+}$ × *Tak1*$^{f/f}$ × *Ripk3*$^{-/-}$ × *Casp8*$^{-/-}$; Fig. 5 A and Fig. S5 A). However, the same LPS + z-VAD stimulation induced necroptotic cell death in *Lyz2*$^{cre+}$ × *Tak1*$^{f/f}$ × *Ripk1*$^{KD/KD}$ BMDMs (Fig. 5 A), revealing that TAK1 deficiency alleviates the requirement for RIPK1 kinase activity to induce necroptosis. To further corroborate the RIPK1 kinase activity–independent form of necroptotic cell death, we analyzed BMDMs for MLKL phosphorylation and oligomerization, the biochemical markers of necroptosis. Western blot analysis showed phosphorylation and oligomerization of MLKL in *Lyz2*$^{cre+}$ × *Tak1*$^{f/f}$ × *Ripk1*$^{KD/KD}$ after LPS + z-VAD or TNF + z-VAD stimulation (Fig. 5 B and Fig. S5 B), demonstrating the occurrence of RIPK1 kinase activity–independent necroptosis in TAK1-deficient macrophages.

TAK1 deficiency bypasses the requirement for RIPK1 kinase activity but not RIPK3 to drive necroptosis

Since our data from the *Lyz2*$^{cre+}$ × *Tak1*$^{f/f}$ × *Ripk3*$^{-/-}$ × *Casp8*$^{-/-}$ and *Ripk3*$^{-/-}$ × *Casp8*$^{-/-}$ mice (Fig. 5, Fig. S3, and Fig. S5, A and B) showed a requirement for RIPK3 and capase-8 to drive cell death under the conditions of TLR priming and caspase inactivation, we further examined the role of RIPK3 in driving necroptosis in TAK1-deficient cells. To determine whether RIPK3 is required for necroptosis induction in TLR-primed TAK1-deficient cells, we stimulated BMDMs with LPS + z-VAD, which induced robust cell death and MLKL phosphorylation in *Lyz2*$^{cre+}$ × *Tak1*$^{f/+}$, *Lyz2*$^{cre+}$ × *Tak1*$^{f/f}$, and *Lyz2*$^{cre+}$ × *Tak1*$^{f/f}$ × *Ripk1*$^{KD/KD}$ cells (Fig. 6, A and B). However, cell death and MLKL activation were not detected in BMDMs from *Lyz2*$^{cre+}$ × *Tak1*$^{f/f}$ × *Ripk3*$^{-/-}$ or *Lyz2*$^{cre+}$ × *Tak1*$^{f/f}$ × *Ripk1*$^{KD/KD}$ × *Ripk3*$^{-/-}$ BMDMs. As expected, TLR stimulation with LPS resulted in robust cell death (Fig. 6 A) and also induced proteolytic activation of caspase-1, caspase-8, and gasdermin D in *Lyz2*$^{cre+}$ × *Tak1*$^{f/f}$, *Lyz2*$^{cre+}$ × *Tak1*$^{f/f}$ × *Ripk1*$^{KD/KD}$, and *Lyz2*$^{cre+}$ × *Tak1*$^{f/f}$ × *Ripk3*$^{-/-}$ BMDMs (Fig. 6 C). Moreover, TLR stimulation also promoted robust cell death and caspase-1, caspase-8, and gasdermin D activation in TAK1-deficient BMDMs that lack both RIPK3 and RIPK1 kinase activity (*Lyz2*$^{cre+}$ × *Tak1*$^{f/f}$ × *Ripk1*$^{KD/KD}$ × *Ripk3*$^{-/-}$; Fig. 6, A and C). Together, these results demonstrate that the requirement of RIPK3 for necroptosis activation is not altered by TLR priming and that TAK1-deficient cells can be rescued from cell death by combined inactivation of necroptosis and caspase-mediated cell death pathways.

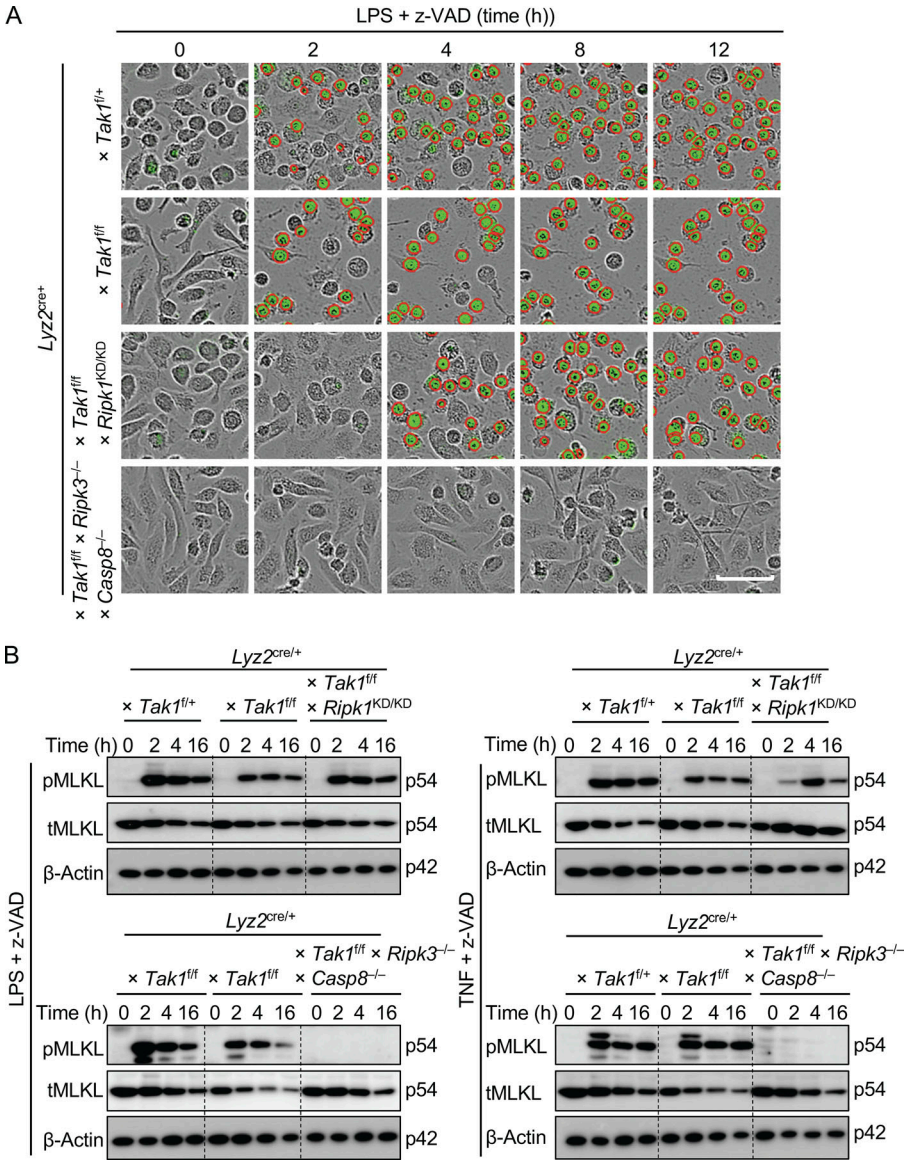

Figure 5. **Priming reveals RIPK1 kinase activity–independent MLKL activation and necroptosis in TAK1-deficient cells. (A)** IncuCyte image analysis of necroptosis induced by LPS + z-VAD treatment of BMDMs. BMDMs were obtained from *Lyz2*$^{cre+}$ × *Tak1*$^{f/+}$, *Lyz2*$^{cre+}$ × *Tak1*$^{f/f}$, *Lyz2*$^{cre+}$ × *Tak1*$^{f/f}$ × *Ripk1*$^{KD/KD}$, and *Lyz2*$^{cre+}$ × *Tak1*$^{f/f}$ × *Ripk3*$^{-/-}$ × *Casp8*$^{-/-}$ mice. Green with red circles indicates dead-cell positivity for the SYTOX Green stain. Scale bar, 50 µm. **(B)** Western blot analysis of the active phosphorylated MLKL (pMLKL) and total MLKL (tMLKL) in the BMDMs treated with LPS + z-VAD (left panel) or TNF + z-VAD (right panel). BMDMs were assessed at the indicated times after treatment in culture. The "p" in Western blots denotes protein molecular weight. Data are representative of two independent experiments with four (A) or two (B) technical replicates for each sample.

RIPK3–caspase-8 axis drives myeloid proliferation in *Lyz2*$^{cre+}$ × *Tak1*$^{f/f}$ mice and the inflammatory pathology during TAK1 inhibition–induced sepsis

Lyz2cre-mediated cell-specific deletion of TAK1 in mice induces myeloid proliferation that is hallmarked by an increase in the neutrophil population in the blood (Ajibade et al., 2012; Lamothe et al., 2012; Malireddi et al., 2018). This neutrophilia is partially rescued in RIPK1 kinase-dead, TAK1-deficient mice (Malireddi et al., 2018). However, it is not clear if the hyperactivated RIPK3 and/or caspase-8 drive this disease in TAK1-deficient mice. Moreover, to further extend our in vitro observations, we investigated the role of the RIPK3–caspase-8 axis in driving the peripheral blood neutrophilia seen in TAK1-deficient mice. Consistent with other studies (Orning et al., 2018; Sarhan et al., 2018) and our in vitro cell death observations, RIPK3 deficiency in TAK1-deficient mice (*Lyz2*$^{cre+}$ × *Tak1*$^{f/f}$ × *Ripk3*$^{-/-}$) did not rescue this neutrophilia; however, RIPK3 and caspase-8 double-deficiency (*Lyz2*$^{cre+}$ × *Tak1*$^{f/f}$ × *Ripk3*$^{-/-}$ × *Casp8*$^{-/-}$) restored the neutrophil frequency and numbers to those of control mice (Fig. 7 A). Hyperinflammation is often associated with the pathophysiology of neutrophilic diseases, and inactivation of MAPKs such as TAK1 exacerbate inflammatory responses that promote neutrophilia and sepsis (Ajibade et al., 2012; Meinzer et al., 2012; Orth et al., 1999; Peterson et al., 2017). To study this phenomenon, we developed a physiologically relevant model of TAK1-i–induced sepsis (Fig. 7 B). To examine the physiological relevance of RIPK1 kinase activity and caspase-8 in vivo, we treated WT, *Ripk1*$^{KD/KD}$, *Ripk3*$^{-/-}$, and *Ripk3*$^{-/-}$ × *Casp8*$^{-/-}$ double-knockout (DKO) mice with an extremely mild, nonlethal dose of LPS (10 µg/mouse) in the presence of TAK1-i. This combination resulted in sensitization and susceptibility of WT mice to low-dose LPS treatment and the development of sepsis-like shock resulting in the death of 60% of the WT mice. However, *Ripk1*$^{KD/KD}$ mice showed significant protection from TAK1-i + LPS-induced septic shock (Fig. 7 C), indicating a role for RIPK1 kinase activity in acute inflammatory responses in this model. In concurrence with the in vitro findings, *Ripk3*$^{-/-}$ × *Casp8*$^{-/-}$ DKO mice were fully protected from this sepsis-like shock (Fig. 7 C).

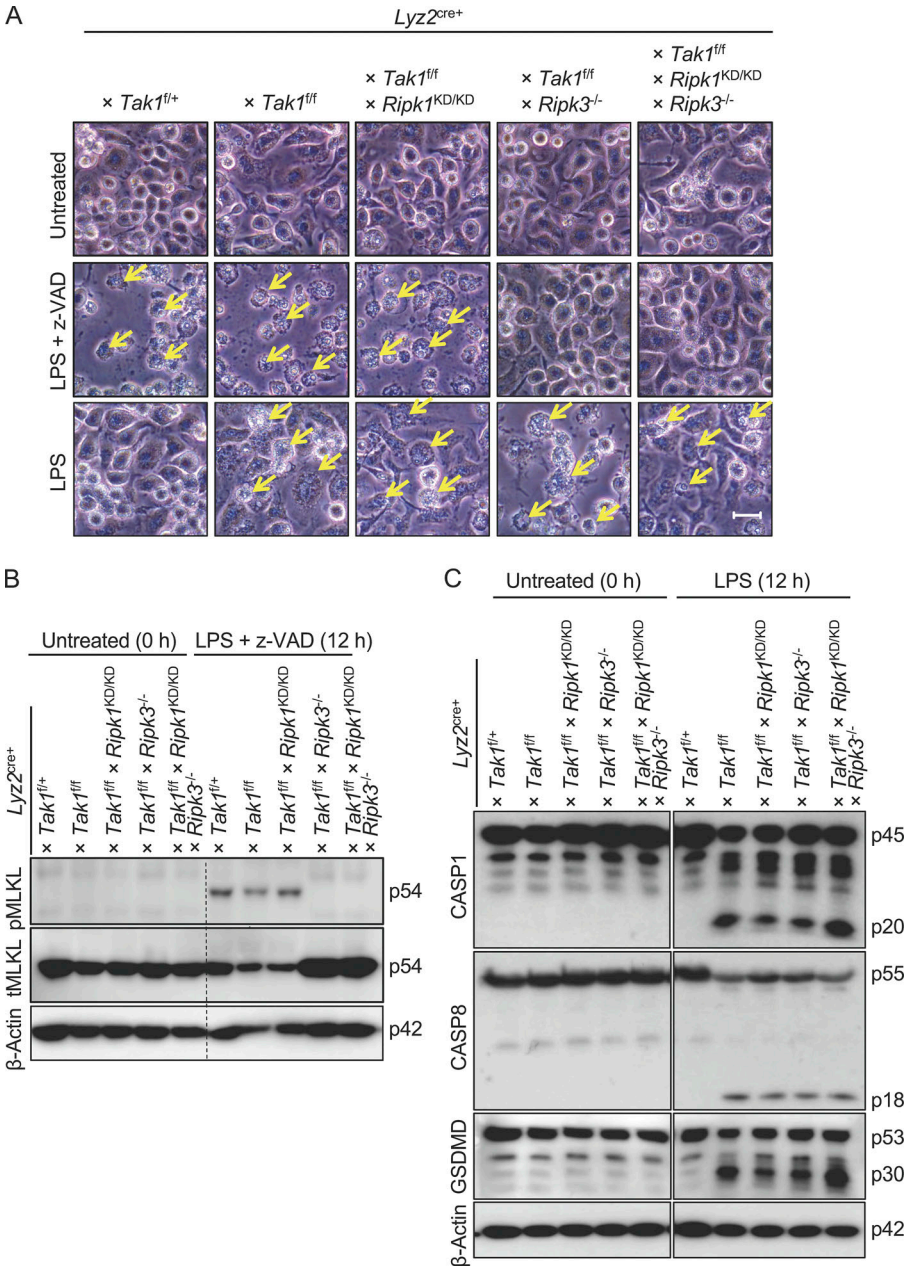

Figure 6. **RIPK3 is required for necroptosis induction in TAK1-deficient cells. (A)** Light microscopic image analysis of cell death induced by LPS or LPS + z-VAD treatment of BMDMs. BMDMs were obtained from *Lyz2*$^{cre+}$ × *Tak1*$^{f/+}$, *Lyz2*$^{cre+}$ × *Tak1*$^{f/f}$, *Lyz2*$^{cre+}$ × *Tak1*$^{f/f}$ × *Ripk1*$^{KD/KD}$, *Lyz2*$^{cre+}$ × *Tak1*$^{f/f}$ × *Ripk3*$^{-/-}$, and *Lyz2*$^{cre+}$ × *Tak1*$^{f/f}$ × *Ripk1*$^{KD/KD}$ × *Ripk3*$^{-/-}$ mice. Yellow arrows indicate dead cells. Scale bar, 50 µm. **(B)** Western blot analysis of the active phosphorylated MLKL (pMLKL) and total MLKL (tMLKL) in the untreated and LPS + z-VAD–treated BMDMs. **(C)** Western blot analysis of the activated caspase-1 subunit p20, caspase-8 subunit p18, and gasdermin D (GSDMD) subunit p30 measured from untreated and LPS-primed BMDMs at 12 h after stimulation. The "p" in Western blots denotes protein molecular weight. Data are representative of two independent experiments with at least two technical replicates per sample.

Liver sections from *Ripk3*$^{-/-}$ × *Casp8*$^{-/-}$ DKO mice consistently lacked signs of inflammation and were protected from neutrophilic infiltration (Fig. S5 C). Deficiency of FADD, an upstream activating adaptor of caspase-8, also provided similar protection from organ damage during TAK1-i + LPS treatment in mice (Fig. S5 C). Furthermore, we found that lack of TAK1 in myeloid cells (*Lyz2*$^{cre+}$ × *Tak1*$^{f/f}$) enhanced susceptibility to LPS-induced septic shock (Fig. 7 D). Lack of RIPK1 kinase activity resulted in partial rescue of the mice, while the combined deletion of RIPK3 and caspase-8 provided full protection from sepsis-induced death (Fig. 7 D). These results support that TAK1 inactivation in myeloid cells relieves the requirement for RIPK1 kinase activity but does require RIPK3 and caspase-8 to drive cell death and inflammation. Together, these studies demonstrate that ripoptosome components caspase-8 and FADD play central roles in promoting myeloid proliferation and severe sepsis in the absence of TAK1.

Discussion

TAK1 is required for NF-κB and MAPK signaling downstream of several pattern-recognition receptors, growth receptors, and cytokine receptors (Ajibade et al., 2013; Dai et al., 2012). We previously described a paradoxical role for TAK1 in restricting RIPK1 kinase activity–dependent NLRP3 inflammasome activation and regulation of cellular homeostasis (Malireddi et al., 2018).

Recent studies have further affirmed the occurrence of RIPK1 kinase activity–dependent pyroptosis under the conditions of *Yersinia*-mediated TAK1 inactivation (Orning et al., 2018; Sarhan et al., 2018). Previously, we have also demonstrated that RIPK1

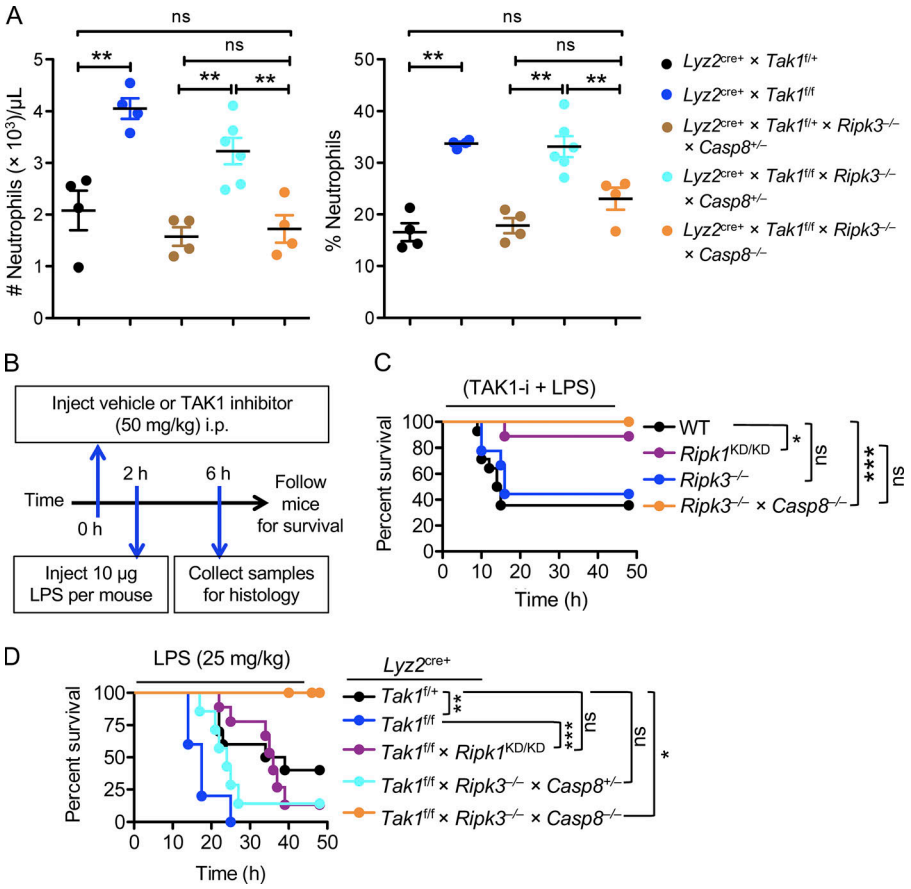

Figure 7. **Caspase-8 deficiency rescues TAK1-deficient mice from myeloid proliferation and sepsis. (A)** Complete blood count analysis of peripheral blood samples from *Lyz2*$^{cre+}$ × *Tak1*$^{f/+}$ (n = 4), *Lyz2*$^{cre+}$ × *Tak1*$^{f/f}$ (n = 4), *Lyz2*$^{cre+}$ × *Tak1*$^{f/+}$ × *Ripk3*$^{-/-}$ × *Casp8*$^{+/-}$ (n = 4), *Lyz2*$^{cre+}$ × *Tak1*$^{f/f}$ × *Ripk3*$^{-/-}$ × *Casp8*$^{+/-}$ (n = 6), and *Lyz2*$^{cre+}$ × *Tak1*$^{f/f}$ × *Ripk3*$^{-/-}$ × *Casp8*$^{-/-}$ (n = 4) mice. Littermate controls used for the experiments included *Tak1*$^{f/f}$ and *Lyz2*$^{cre+}$ × *Tak1*$^{f/+}$ mice. All data are presented as the mean ± SEM, and each dot represents a single mouse. **(B)** Schematic showing experimental design of the LPS + TAK1-i–induced septic shock model. **(C)** Survival analysis of 8-wk-old WT mice (n = 14), *Ripk1*$^{KD/KD}$ (n = 9), *Ripk3*$^{-/-}$ mice (n = 9), and *Ripk3*$^{-/-}$ × *Casp8*$^{-/-}$ mice (n = 12) in the LPS + TAK1-i–induced septic shock model. **(D)** Survival analysis of control *Lyz2*$^{cre+}$ × *Tak1*$^{f/+}$ (n = 10), *Lyz2*$^{cre+}$ × *Tak1*$^{f/f}$ (n = 5), *Lyz2*$^{cre+}$ × *Tak1*$^{f/f}$ × *Ripk1*$^{KD/KD}$ (n = 9), *Lyz2*$^{cre+}$ × *Tak1*$^{f/f}$ × *Ripk3*$^{-/-}$ × *Casp8*$^{+/-}$ (n = 7), and *Lyz2*$^{cre+}$ × *Tak1*$^{f/f}$ × *Ripk3*$^{-/-}$ × *Casp8*$^{-/-}$ mice (n = 6) in the LPS-induced septic shock model. Statistical significance between groups was determined by Mann-Whitney test (A) or log-rank (Mantel-Cox) test (C and D), and P values < 0.05 were considered statistically significant. ns, not significant; *, P < 0.05; **, P < 0.01; ***, P < 0.001. Data are representative of three (A) or two (C and D) independent experiments.

kinase activity promotes neutrophilic dermatosis in the spontaneous *Ptpn6*^{spin} mouse model of the inflammatory syndrome (Lukens et al., 2013). However, here we investigated the molecular mechanisms that govern cell death and inflammation under TAK1-deficient conditions that would occur in the presence of PAMPs to model pathogenic insults. We found an association of RIPK1 with NLRP3 and ASC and a priming-independent role for caspase-8 and FADD in driving inflammasome activation and cell death in TAK1-deficient BMDMs. We also discovered the existence of RIPK1 kinase activity–independent inflammatory cell death and inflammasome activation. Our findings suggest that RIPK1 kinase inhibition may not successfully treat disorders associated with TAK1 dysfunction when TLRs are stimulated (such as by the microbiome, infection, or damage). Although microbes have evolved to inactivate central nodes of inflammatory signaling, such as TAK1 and other MAPKs, to modulate the host immune response, host coevolution has opted to sense these intracellular insults to promote alternative modes of immune activation and inflammatory cell death (Ajibade et al., 2012; Meinzer et al., 2012; Orth et al., 1999; Peterson et al., 2017). Our current findings show an alternate pathway of ripoptosome-like, but RIPK1 kinase activity–dependent and –independent mechanisms to drive inflammatory cell death, which may also contribute to the pathophysiology of some inflammatory diseases and sepsis.

The differences in the kinase and scaffold functions of RIPK1 have been well studied. The scaffolding function (through K63-linked polyubiquitination) is required to recruit TNF receptor–associated factor 2 (TRAF2), cellular inhibitor of apoptosis proteins, TAK1, and TGF-β–activated kinase and MAP3K7 binding protein 2 (TAB2) to stabilize complex-I, which promotes the activation of NF-κB and ERK signaling (Ea et al., 2006; Lee et al., 2004). In the absence of complex-I components, ligation of TNFR1 or TLRs leads to RIPK1 kinase-dependent recruitment of FADD and caspase-8, which assembles complex-II to promote apoptosis; however, as a backup mechanism of cell death, complex-II can also drive RIPK3-MLKL–mediated necroptosis when caspases are inhibited (Feoktistova et al., 2011; Tenev et al., 2011). Thus, the RIPK1 scaffold function promotes prosurvival signaling, whereas RIPK1 kinase activity is important for inducing RIPK1-mediated cell death. RIPK1 plays central roles in regulating cell death and inflammation, which is particularly important to promote immune defense against pathogenic microbes such as *Yersinia* species. Our data provide evidence for the presence of a novel cell death mechanism and support the concept that cells have evolved to sense TAK1 inactivation as a danger signal to drive RIPK1 kinase activity–independent modes of cell death to bypass the pathogen-mediated immune evasion strategies. However, under these conditions, it is also possible that microbial PAMPs may prime an unknown serine/threonine kinase that substitutes for RIPK1 kinase activity in activating downstream target molecules for cell death induction. Alternatively, TLR priming may promote direct RIPK1 phosphorylation, ubiquitination, or a transition to an open conformation that facilitates its role as a scaffold protein to induce cell death. In line with this hypothesis, we found that TLR priming accelerated

cell death in TAK1-deficient BMDMs, but more importantly, it promoted cell death of TAK1-deficient BMDMs even in the absence of RIPK1 kinase activity. Specifically, LPS stimulation promoted cell death in *Lyz2*$^{cre+}$ × *Tak1*$^{f/f}$ × *Ripk1*$^{KD/KD}$ BMDMs. A recent report described that TAK1-deficient macrophages undergo a partially RIPK1 kinase activity–independent form of inflammatory cell death (Sanjo et al., 2019), complementing our results. We observed a significant role for RIPK1 kinase activity in TAK1-i + LPS–induced septic shock, supporting its role in driving acute inflammatory responses in this model. These findings also reflect the delayed cell death observed in TAK1-i + LPS–treated *Ripk1*$^{KD/KD}$ BMDMs, suggesting that the delayed myeloid cell death may contribute to the protection from septic shock. Alternatively, it is also highly likely that the TAK1-i targets other nonmyeloid cells, which would not be affected in the myeloid-specific *Lyz2*$^{cre+}$ × *Tak1*$^{f/f}$ mice. Therefore, the hypersusceptibility to sepsis in this case is a result of combined responses coming from both the myeloid and nonmyeloid cells. However, we observed that genetic deletion of TAK1 in myeloid cells (*Lyz2*$^{cre+}$ × *Tak1*$^{f/f}$) augmented the susceptibility to LPS-induced septic shock and was only partially dependent on RIPK1 kinase activity compared with the combined deletion of RIPK3 and caspase-8, which provided complete protection in this model. These results support that TAK1 inactivation in myeloid cells relieves the requirement for RIPK1 kinase activity but not RIPK3 and caspase-8 to drive cell death and inflammation. We further extended these findings using RIPK1-deficient fetal liver–derived macrophages, which demonstrated a requirement for RIPK1 scaffold function, while RIPK1 kinase activity is dispensable for cell death and inflammasome activation under TAK1-deficient conditions. The upstream mechanisms acting on RIPK1 to drive the scaffold-mediated cell death observed in LPS-stimulated *Lyz2*$^{cre+}$ × *Tak1*$^{f/f}$ × *Ripk1*$^{KD/KD}$ BMDMs are not known and warrant further investigation. Regardless, our data highlight a RIPK1 kinase activity–independent, ripoptosome-like cell death complex that drives inflammasome activation and cell death in TAK1-deficient cells.

TAK1-deficient BMDMs undergo spontaneous forms of cell death that include apoptosis, pyroptosis, and the alternative backup process of necroptosis (Malireddi et al., 2018). Recent findings have highlighted the importance of homeostatic regulation of RIPK1 in preventing cell death and the development of inflammatory diseases such as amyotrophic lateral sclerosis, and multiple MAPKs coordinate to restrain spontaneous RIPK1 activation by mediating inhibitory phosphorylation of this kinase (Dondelinger et al., 2015; Geng et al., 2017; Jaco et al., 2017; Xu et al., 2018). Pharmacological inactivation of TAK1 also drives RIPK1 kinase-dependent apoptosis (Amin et al., 2018). We observed that caspase-8 was associating with inflammasome components in TAK1-deficient BMDMs and was important for inflammasome activation under both unprimed and primed conditions. Importantly, TLR priming bypassed the requirement for RIPK1 kinase activity and promoted cell death and inflammasome activation in *Lyz2*$^{cre+}$ × *Tak1*$^{f/f}$ × *Ripk1*$^{KD/KD}$ BMDMs. Moreover, a recent study showed that caspase-8–mediated cleavage of RIPK1 is essential for limiting aberrant cell death and loss of developmental homeostasis (Newton et al., 2019). Interestingly, they observed that *Ripk1*$^{D138N,D325A/D138N,D325A}$ mice that lack both RIPK1 kinase activity and sites for cleavage by caspase-8 were runted and did not survive to weaning age, suggesting a kinase activity–independent role for RIPK1 in cell death, which complements our findings. Thus, both the kinase-dependent and -independent functions of RIPK1 drive inflammatory cell death.

In summary, using TAK1-deficient cells, we have uncovered a previously unknown role for RIPK1 kinase activity–dependent and –independent functions in promoting multifaceted cell death complex formation, which drives activation of the NLRP3 inflammasome, pyroptosis, apoptosis, and necroptosis, referred to as PANoptosis (Malireddi et al., 2019). The occurrence of RIPK1 kinase activity–independent necroptosis in TAK1-deficient macrophages provides a novel model to further explore the alternative cellular mechanisms of MLKL and/or RIPK3 activation with potential implications for inflammatory cell death and disease. Future studies should address how TLR priming during TAK1 deficiency bypasses the requirement for RIPK1 to induce necroptosis. Together, our findings highlight the complexity in regulating inflammatory cell death and identify potential factors that could be targeted to treat myeloid proliferation and sepsis.

Materials and methods

Experimental animal models and subject details

Mice

Ripk1$^{-/-}$ (Kelliher et al., 1998); *Ripk3*$^{-/-}$ (Newton et al., 2004); *Mlkl*$^{-/-}$, *Ripk3*$^{-/-}$ × *Fadd*$^{-/-}$, and *Ripk3*$^{-/-}$ × *Casp8*$^{-/-}$ (Gurung et al., 2014; Oberst et al., 2011); *Nlrp3*$^{-/-}$ (Kanneganti et al., 2006); and *Lyz2*$^{cre+}$ × *Tak1*$^{f/f}$ × *Nlrp3*$^{-/-}$ (Malireddi et al., 2018) mouse strains were all described previously. *Tak1*$^{f/f}$ mice were bred with *Lyz2*$^{cre+}$ (*B6.129P2-Lyz2*$^{tm1(cre)Ifo}$*/J*; The Jackson Laboratory) mice to generate conditional TAK1-knockout mice. TAK1-knockout mice were bred with *Ripk1*$^{KD/KD(K45A)}$ mice (generated in this study and described below), *Mlkl*$^{-/-}$, *Ripk3*$^{-/-}$, or *Ripk3*$^{-/-}$ × *Casp8*$^{-/-}$ mice to generate *Lyz2*$^{cre+}$ × *Tak1*$^{f/f}$ × *Ripk1*^{K45A} (*Ripk1*$^{KD/KD}$), *Lyz2*$^{cre+}$ × *Tak1*$^{f/f}$ × *Mlkl*$^{-/-}$, *Lyz2*$^{cre+}$ × *Tak1*$^{f/f}$ × *Ripk3*$^{-/-}$, *Lyz2*$^{cre+}$ × *Tak1*$^{f/f}$ × *Ripk1*$^{KD/KD}$ × *Ripk3*$^{-/-}$, and *Lyz2*$^{cre+}$ × *Tak1*$^{f/f}$ × *Ripk3*$^{-/-}$ × *Casp8*$^{-/-}$ mice. C57BL/6 WT (The Jackson Laboratory) and littermate controls were bred at St. Jude Children's Research Hospital (St. Jude). Animal studies were conducted under protocols approved by the St. Jude Animal Care and Use Committee.

Generation of the Ripk1^{K45A} (Ripk1$^{KD/KD}$) *mouse strain*

Ripk1^{K45A} mice were generated using CRISPR/Cas9 technology. Staff in the St. Jude Transgenic/Gene Knockout Shared Resource injected pronuclear-staged C57BL/6J zygotes with a single-guide RNA (sgRNA; Ripk1_K45A_Guide 01, 5′-TCCTGAAAAAAGTAT ACACA-3′; 125 ng/µl) designed to introduce a DNA double-stranded break into exon 2 of the *Ripk1* gene, human codon-optimized *Cas9* mRNA transcripts (50 ng/µl), and a 200-nucleotide single-stranded DNA molecule containing the desired mutations (Ripk1–K45A–HDR [homology-directed repair], 5′-AGGCTTCGGGAAGGTGTCCTTGTGTTACCACAGAAGCCA TGGATTTGTCATCCTGGCGAAAGTCTACACCGGTCCCAACCG CGCTGAGTGAGTTGGGGGCATAAAGGGCTTGGCTTTTTGCTA GCTGAC-3′; Fig. S1). To facilitate the identification of founder mice and genotyping, silent substitutions generating an AgeI

restriction site (5′-ACCGGT-3′) were also introduced. Zygotes were surgically transplanted into the oviducts of pseudopregnant CD1 females, and newborn mice carrying the *Ripk1*^{K45A} allele were identified by PCR, AgeI-restriction digestion, and Sanger sequencing using primers Ripk1-K45A-F51 (5′-CGGTCCTTTTGCCCTGAGAC-3′) and Ripk1-K45A-R52 (5′-AAAAAGGCGCCCCTCTCAA-3′). The sgRNAs and *Cas9* mRNA transcripts were designed and generated as described previously (Pelletier et al., 2015). The target site for each sgRNA is unique in the mouse genome, and no potential off-target site with fewer than three mismatches was found using the Cas-OFFinder algorithm (Bae et al., 2014).

Macrophage differentiation and stimulation

BMDMs were differentiated from bone marrow cells as detailed previously (Gurung et al., 2012). In brief, cells isolated from bone marrow were maintained in culture in L929 cell-conditioned IMDM supplemented with 10% fetal bovine serum, 1% nonessential amino acids, and 1% penicillin–streptomycin for 5 d to differentiate into macrophages. Fully differentiated BMDMs were collected on day 5 and seeded into 12-well cell culture plates. As indicated for pharmacologic inhibition, BMDMs were treated before or after stimulation with chemical inhibitors of inflammatory signaling or cell death. In other experiments, BMDMs were treated with the TAK1-i 5Z-7-oxozeaenol (0.1 µM), Pam3CSK4 (10 µg/ml), poly(I:C) (10 µg/ml), or mTNF (50 ng/ml) or infected with *Y. enterocolitica* (ATCC 700822) at a multiplicity of infection (MOI) of 5 to study inflammasome activation and cell death.

Bacterial culture and stimulation

Y. enterocolitica was grown on 2× yeast extract tryptone (YT) agar plates overnight under aerobic conditions at 37°C. Next, single colonies were cultured in the 2× YT broth overnight at 26°C. Then the bacteria were subcultured (1:10) in fresh 2× YT broth for 2 h and washed and resuspended in PBS for infection of BMDMs. Extracellular bacteria were killed by adding gentamicin (100 µg/ml) 1 h after infection.

Analysis of neutrophilia and TAK1-i–induced inflammatory septic shock in vivo

The neutrophilia phenotype was assessed in vivo by a standard complete blood count performed on an automated laboratory instrument. Peripheral blood samples were collected in EDTA (1% wt/vol) from *Lyz2*$^{cre+}$ × *Tak1*$^{f/+}$, *Lyz2*$^{cre+}$ × *Tak1*$^{f/f}$, *Lyz2*$^{cre+}$ × *Tak1*$^{f/+}$ × *Ripk3*$^{-/-}$ × *Casp8*$^{+/-}$, *Lyz2*$^{cre+}$ × *Tak1*$^{f/f}$ × *Ripk3*$^{-/-}$ × *Casp8*$^{+/-}$, and *Lyz2*$^{cre+}$ × *Tak1*$^{f/f}$ × *Ripk3*$^{-/-}$ × *Casp8*$^{-/-}$ mice. For in vivo septic shock treatments, WT or genetically manipulated knockout mice were intraperitoneally injected with TAK1-i (50 mg/kg body weight) followed by LPS (10 µg) 2 h later, or alternatively mice were subjected to standard LPS shock (25 mg/kg body weight). Tissue samples were collected 6 h after completion of TAK1-i treatment for histological analysis of inflammation and cell death, or the mice were monitored for an extended period (50 h) for survival analysis.

Western blotting

Protein samples for Western blotting were prepared by collecting and combining cell lysates with cell culture supernatants. Samples were denatured by boiling for 10 min at 100°C in loading buffer containing 10% SDS and 100 mM dithiothreitol. SDS-PAGE–separated proteins were transferred to Amersham Hybond P polyvinylidene difluoride membranes (10600023; GE Healthcare Life Sciences) and immunoblotted with primary antibodies against caspase-1 (mouse mAb, Casper-1, AG-20B-0042; AdipoGen Life Sciences), caspase-3 (rabbit polyclonal antibody [pAb], 9662; Cell Signaling Technology), cleaved caspase-3 (rabbit pAb, 9661; Cell Signaling Technology), gasdermin D (rabbit mAb, ab209845; Abcam), ASC (rabbit pAb, AL177, AG-25B-0006; AdipoGen Life Sciences), RIPK1 (rabbit mAb, 3493; Cell Signaling Technology or mouse anti-RIP clone 38/RIP, 610458; BD Biosciences), caspase-8 (rat mAb, clone 1G12, AG-20T-0137; AdipoGen Life Sciences), cleaved caspase-8 (rabbit mAb, Asp391, 9496; Cell Signaling Technology), MLKL (rabbit pAb, AP14272b; Abgent), phospho-MLKL (rabbit mAb, 37333; Cell Signaling Technology), NLRP3 (mouse mAb, Cryo-2, AG-20B-0014; AdipoGen Life Sciences), or β-actin (rabbit mAb, 13E5, 4970; Cell Signaling Technology) followed by secondary anti-rabbit, anti-mouse, or anti-rat HRP antibodies (Jackson ImmunoResearch Laboratories), as previously described (Kanneganti et al., 2006).

Immunoprecipitation

For protein–protein interaction studies, cell lysates prepared in NP-40 lysis buffer (1.0% NP-40, 150 mM NaCl, and 50 mM HEPES) containing complete protease inhibitors and phospho-STOP (Roche) were subjected to immunoprecipitation with 3 µg/sample of the indicated primary antibodies that were cross-linked to Dynabeads (Superparamagnetic Dynabeads M-270; Thermo Fisher Scientific) on a rocking platform for 12 to 16 h at 4°C. After the incubation, the beads were centrifuged and washed three times with the lysis buffer. Immunoprecipitates were eluted in sample buffer after three washes in the 2× SDS loading buffer and then subjected to immunoblotting analysis.

Light microscopy and histology

BMDMs from WT and the indicated knockout mice were seeded in 12-well cell culture plates and were either left untreated (control) or treated with TAK1-i or different inhibitors of inflammation or cell death for the indicated times. Light microscopy images were obtained using an Olympus CKX41 microscope with a 40× objective lens. Digital image recording and analysis were performed with the INFINITY ANALYZE software (Lumenera Corporation). The images were processed and analyzed with ImageJ software. For histological analysis, livers were fixed in 10% formalin, embedded in paraffin, sectioned, and stained with hematoxylin and eosin. A board-certified pathologist analyzed the stained sections for the presence of inflammation and signs of tissue damage in a blinded manner.

Fluorescence microscopy

Unprimed or primed BMDMs were fixed for 5 min at room temperature in 4% ChemCruz paraformaldehyde (sc-281692; Santa Cruz Biotechnology). The cells were permeabilized and blocked for nonspecific binding with 10% normal goat serum

(Sigma-Aldrich) in PBS containing 0.1% Triton X-100. Cells were incubated with the following primary antibodies overnight at 4°C or for 2 h at room temperature: anti-ASC (rabbit pAb AL177; diluted 1:200; AdipoGen Life Sciences), anti-RIPK1 (mouse anti-RIP clone 38/RIP; diluted 1:50; BD Biosciences), or anti–caspase-8 (rat mAb clone 1G12; diluted 1:100; AdipoGen Life Sciences). The secondary antibodies used were an Alexa Fluor 594–conjugated antibody against rat immunoglobulin G (A-11007; diluted 1:250; Life Technologies), an Alexa Fluor 568–conjugated antibody against rabbit immunoglobulin G (A-11011; diluted 1:250; Life Technologies), and an Alexa Fluor 488–conjugated antibody against mouse immunoglobulin G (R37120; diluted 1:250; Life Technologies). Cells were counterstained with DAPI mounting medium (Vector Laboratories), and confocal microscopy was performed using an AxioObserverZ.1 inverted microscope (Zeiss) equipped with a CSU-X spinning disc (Yokagawa), 100× (1.45 numerical aperture) objective, and Prime 95B complementary metal oxide semiconductor camera (Teledyne Photometrics). Images were acquired and analyzed using Slidebook software (Intelligent Imaging Innovations).

IncuCyte cell death analysis

Time-course analysis of cell death assays was performed using a two-color IncuCyte Zoom in incubator imaging system (Essen Biosciences). Fully differentiated BMDMs were seeded in 12-well (1.0×10^6 cells/well) or 24-well (0.5×10^6 cells/well) tissue culture vessels in the presence of 100 nM of the cell-impermeable DNA binding fluorescent dye SYTOX Green (S7020; Life Technologies), which rapidly enters dying cells during membrane permeabilization. A series of images were acquired with a 20× objective and analyzed using the IncuCyte S3 software, which allows precise analysis of the number of SYTOX Green–positive cells present in each image. A minimum of three images per well was taken for the analysis of each time point. Dead-cell events for each strain of BMDMs were acquired via SYTOX Green staining and plotted using GraphPad Prism version 5.0 software.

Statistical analysis

GraphPad Prism version 5.0 software was used for data analysis. Data are shown as mean ± SEM. Statistical significance was determined by *t* tests (two-tailed) for two groups, log-rank (Mantel-Cox) test for survival analysis, and one-way ANOVA (with Dunnett's or Tukey's multiple comparisons tests) for three or more groups. The number of repeats for each experiment is indicated in the corresponding figure legends; *n* in the figure legends represents the number of animals used in the experiments. $P < 0.05$ was considered statistically significant and is represented as *; ns, not significant.

Online supplemental material

Fig. S1 shows generation of *Ripk1*$^{KD/KD}$ mice by using CRISPR/Cas9 technology. Fig. S2 shows that priming via TLR2 or TLR3 or by *Y. enterocolitica* bypasses the requirement for RIPK1 kinase activity in promoting cell death and caspase-1 activation. Fig. S3 shows that during TAK1 inactivation, FADD and caspase-8 are required for cell death and inflammasome activation, both in the presence and in the absence of priming. Fig. S4 shows that genetic deletion of RIPK3 and caspase-8 protects TAK1-deficient cells from cell death, both in the presence and in the absence of priming. Fig. S5 shows that genetic deletion of caspase-8 rescues TAK1 inactivation–induced inflammatory cell death of myeloid cells and that FADD deletion rescues TAK1-deficient mice from the pathophysiology of sepsis.

Acknowledgments

We thank Dr. Hongbo Chi (St. Jude Children's Research Hospital, Memphis, TN) for generously supplying TAK1-mutant mice and Rebecca Tweedell, PhD, for scientific editing and writing support.

T.-D. Kanneganti is supported by funding from the National Institutes of Health (grants AI101935, AI124346, AR056296, and CA163507) and the American Lebanese Syrian Associated Charities. P. Gurung is supported by the National Institute of Allergy and Infectious Diseases (grant K22AI127836) and the National Institute of Environmental Health Sciences (P30ES005605 pilot grant) and by University of Iowa startup funds.

Author contributions: R.K.S. Malireddi, P. Gurung, and T.-D. Kanneganti designed the study. R.K.S. Malireddi, P. Gurung, S. Kesavardhana, P. Samir, A. Burton, H. Mummareddy, S. Pelletier, and S. Burgula performed the experiments. R.K.S. Malireddi, P. Gurung, and T.-D. Kanneganti analyzed the data with input from the other authors. P. Vogel conducted the histological analysis. R.K.S. Malireddi, P. Gurung, and T.-D. Kanneganti wrote the manuscript with input from the other authors. T.-D. Kanneganti oversaw the project.

Disclosures: The authors declare no competing interests exist.

Submitted: 3 September 2019
Revised: 22 October 2019
Accepted: 18 November 2019

References

Ajibade, A.A., Q. Wang, J. Cui, J. Zou, X. Xia, M. Wang, Y. Tong, W. Hui, D. Liu, B. Su, et al. 2012. TAK1 negatively regulates NF-κB and p38 MAP kinase activation in Gr-1$^+$CD11b$^+$ neutrophils. *Immunity*. 36:43–54. https://doi.org/10.1016/j.immuni.2011.12.010

Ajibade, A.A., H.Y. Wang, and R.F. Wang. 2013. Cell type-specific function of TAK1 in innate immune signaling. *Trends Immunol.* 34:307–316. https://doi.org/10.1016/j.it.2013.03.007

Amin, P., M. Florez, A. Najafov, H. Pan, J. Geng, D. Ofengeim, S.A. Dziedzic, H. Wang, V.J. Barrett, Y. Ito, et al. 2018. Regulation of a distinct activated RIPK1 intermediate bridging complex I and complex II in TNFα-mediated apoptosis. *Proc. Natl. Acad. Sci. USA.* 115:E5944–E5953. https://doi.org/10.1073/pnas.1806973115

Bae, S., J. Park, and J.S. Kim. 2014. Cas-OFFinder: a fast and versatile algorithm that searches for potential off-target sites of Cas9 RNA-guided endonucleases. *Bioinformatics.* 30:1473–1475. https://doi.org/10.1093/bioinformatics/btu048

Dai, L., C. Aye Thu, X.Y. Liu, J. Xi, and P.C. Cheung. 2012. TAK1, more than just innate immunity. *IUBMB Life.* 64:825–834. https://doi.org/10.1002/iub.1078

Dillon, C.P., A. Oberst, R. Weinlich, L.J. Janke, T.B. Kang, T. Ben-Moshe, T.W. Mak, D. Wallach, and D.R. Green. 2012. Survival function of the FADD-CASPASE-8-cFLIP$_L$ complex. *Cell Reports.* 1:401–407. https://doi.org/10.1016/j.celrep.2012.03.010

Dondelinger, Y., S. Jouan-Lanhouet, T. Divert, E. Theatre, J. Bertin, P.J. Gough, P. Giansanti, A.J. Heck, E. Dejardin, P. Vandenabeele, and M.J. Bertrand. 2015. NF-κB-independent role of IKKα/IKKβ in preventing RIPK1

kinase-dependent apoptotic and necroptotic cell death during TNF signaling. *Mol. Cell.* 60:63–76. https://doi.org/10.1016/j.molcel.2015.07.032

Ea, C.K., L. Deng, Z.P. Xia, G. Pineda, and Z.J. Chen. 2006. Activation of IKK by TNFalpha requires site-specific ubiquitination of RIP1 and polyubiquitin binding by NEMO. *Mol. Cell.* 22:245–257. https://doi.org/10.1016/j.molcel.2006.03.026

Feoktistova, M., P. Geserick, B. Kellert, D.P. Dimitrova, C. Langlais, M. Hupe, K. Cain, M. MacFarlane, G. Häcker, and M. Leverkus. 2011. cIAPs block Ripoptosome formation, a RIP1/caspase-8 containing intracellular cell death complex differentially regulated by cFLIP isoforms. *Mol. Cell.* 43:449–463. https://doi.org/10.1016/j.molcel.2011.06.011

Geng, J., Y. Ito, L. Shi, P. Amin, J. Chu, A.T. Ouchida, A.K. Mookhtiar, H. Zhao, D. Xu, B. Shan, et al. 2017. Regulation of RIPK1 activation by TAK1-mediated phosphorylation dictates apoptosis and necroptosis. *Nat. Commun.* 8:359. https://doi.org/10.1038/s41467-017-00406-w

Guo, X., H. Yin, Y. Chen, L. Li, J. Li, and Q. Liu. 2016. TAK1 regulates caspase 8 activation and necroptotic signaling via multiple cell death checkpoints. *Cell Death Dis.* 7:e2381. https://doi.org/10.1038/cddis.2016.294

Gurung, P., R.K. Malireddi, P.K. Anand, D. Demon, L. Vande Walle, Z. Liu, P. Vogel, M. Lamkanfi, and T.D. Kanneganti. 2012. Toll or interleukin-1 receptor (TIR) domain-containing adaptor inducing interferon-β (TRIF)-mediated caspase-11 protease production integrates Toll-like receptor 4 (TLR4) protein- and Nlrp3 inflammasome-mediated host defense against enteropathogens. *J. Biol. Chem.* 287:34474–34483. https://doi.org/10.1074/jbc.M112.401406

Gurung, P., P.K. Anand, R.K. Malireddi, L. Vande Walle, N. Van Opdenbosch, C.P. Dillon, R. Weinlich, D.R. Green, M. Lamkanfi, and T.D. Kanneganti. 2014. FADD and caspase-8 mediate priming and activation of the canonical and noncanonical Nlrp3 inflammasomes. *J. Immunol.* 192:1835–1846. https://doi.org/10.4049/jimmunol.1302839

Human Microbiome Project Consortium. 2012. Structure, function and diversity of the healthy human microbiome. *Nature.* 486:207–214. https://doi.org/10.1038/nature11234

Jaco, I., A. Annibaldi, N. Lalaoui, R. Wilson, T. Tenev, L. Laurien, C. Kim, K. Jamal, S. Wicky John, G. Liccardi, et al. 2017. MK2 phosphorylates RIPK1 to prevent TNF-induced cell death. *Mol. Cell.* 66:698–710.e5. https://doi.org/10.1016/j.molcel.2017.05.003

Kaiser, W.J., J.W. Upton, A.B. Long, D. Livingston-Rosanoff, L.P. Daley-Bauer, R. Hakem, T. Caspary, and E.S. Mocarski. 2011. RIP3 mediates the embryonic lethality of caspase-8-deficient mice. *Nature.* 471:368–372. https://doi.org/10.1038/nature09857

Kanneganti, T.D., N. Ozören, M. Body-Malapel, A. Amer, J.H. Park, L. Franchi, J. Whitfield, W. Barchet, M. Colonna, P. Vandenabeele, et al. 2006. Bacterial RNA and small antiviral compounds activate caspase-1 through cryopyrin/Nalp3. *Nature.* 440:233–236. https://doi.org/10.1038/nature04517

Karki, R., and T.D. Kanneganti. 2019. Diverging inflammasome signals in tumorigenesis and potential targeting. *Nat. Rev. Cancer.* 19:197–214.

Kayagaki, N., I.B. Stowe, B.L. Lee, K. O'Rourke, K. Anderson, S. Warming, T. Cuellar, B. Haley, M. Roose-Girma, Q.T. Phung, et al. 2015. Caspase-11 cleaves gasdermin D for non-canonical inflammasome signalling. *Nature.* 526:666–671. https://doi.org/10.1038/nature15541

Kelliher, M.A., S. Grimm, Y. Ishida, F. Kuo, B.Z. Stanger, and P. Leder. 1998. The death domain kinase RIP mediates the TNF-induced NF-kappaB signal. *Immunity.* 8:297–303. https://doi.org/10.1016/S1074-7613(00)80535-X

Lamothe, B., Y. Lai, L. Hur, N.M. Orozco, J. Wang, A.D. Campos, M. Xie, M.D. Schneider, C.R. Lockworth, J. Jakacky, et al. 2012. Deletion of TAK1 in the myeloid lineage results in the spontaneous development of myelomonocytic leukemia in mice. *PLoS One.* 7:e51228. https://doi.org/10.1371/journal.pone.0051228

Landström, M. 2010. The TAK1-TRAF6 signalling pathway. *Int. J. Biochem. Cell Biol.* 42:585–589. https://doi.org/10.1016/j.biocel.2009.12.023

Lee, T.H., J. Shank, N. Cusson, and M.A. Kelliher. 2004. The kinase activity of Rip1 is not required for tumor necrosis factor-α-induced IkappaB kinase or p38 MAP kinase activation or for the ubiquitination of Rip1 by Traf2. *J. Biol. Chem.* 279:33185–33191. https://doi.org/10.1074/jbc.M404206200

Lukens, J.R., P. Vogel, G.R. Johnson, M.A. Kelliher, Y. Iwakura, M. Lamkanfi, and T.D. Kanneganti. 2013. RIP1-driven autoinflammation targets IL-1α independently of inflammasomes and RIP3. *Nature.* 498:224–227. https://doi.org/10.1038/nature12174

Malireddi, R.K.S., P. Gurung, J. Mavuluri, T.K. Dasari, J.M. Klco, H. Chi, and T.D. Kanneganti. 2018. TAK1 restricts spontaneous NLRP3 activation and cell death to control myeloid proliferation. *J. Exp. Med.* 215:1023–1034. https://doi.org/10.1084/jem.20171922

Malireddi, R.K.S., S. Kesavardhana, and T.D. Kanneganti. 2019. ZBP1 and TAK1: Master regulators of NLRP3 inflammasome/pyroptosis, apoptosis, and necroptosis (PAN-optosis). *Front. Cell. Infect. Microbiol.* 9:406. https://doi.org/10.3389/fcimb.2019.00406

Man, S.M., and T.D. Kanneganti. 2016. Converging roles of caspases in inflammasome activation, cell death and innate immunity. *Nat. Rev. Immunol.* 16:7–21. https://doi.org/10.1038/nri.2015.7

Meinzer, U., F. Barreau, S. Esmiol-Welterlin, C. Jung, C. Villard, T. Léger, S. Ben-Mkaddem, D. Berrebi, M. Dussaillant, Z. Alnabhani, et al. 2012. *Yersinia pseudotuberculosis* effector YopJ subverts the Nod2/RICK/TAK1 pathway and activates caspase-1 to induce intestinal barrier dysfunction. *Cell Host Microbe.* 11:337–351. https://doi.org/10.1016/j.chom.2012.02.009

Mihaly, S.R., J. Ninomiya-Tsuji, and S. Morioka. 2014. TAK1 control of cell death. *Cell Death Differ.* 21:1667–1676. https://doi.org/10.1038/cdd.2014.123

Newton, K., X. Sun, and V.M. Dixit. 2004. Kinase RIP3 is dispensable for normal NF-κ Bs, signaling by the B-cell and T-cell receptors, tumor necrosis factor receptor 1, and Toll-like receptors 2 and 4. *Mol. Cell. Biol.* 24:1464–1469. https://doi.org/10.1128/MCB.24.4.1464-1469.2004

Newton, K., K.E. Wickliffe, D.L. Dugger, A. Maltzman, M. Roose-Girma, M. Dohse, L. Kőműves, J.D. Webster, and V.M. Dixit. 2019. Cleavage of RIPK1 by caspase-8 is crucial for limiting apoptosis and necroptosis. *Nature.* 574:428–431. https://doi.org/10.1038/s41586-019-1548-x

Oberst, A., C.P. Dillon, R. Weinlich, L.L. McCormick, P. Fitzgerald, C. Pop, R. Hakem, G.S. Salvesen, and D.R. Green. 2011. Catalytic activity of the caspase-8-FLIP$_{(L)}$ complex inhibits RIPK3-dependent necrosis. *Nature.* 471:363–367. https://doi.org/10.1038/nature09852

Orning, P., D. Weng, K. Starheim, D. Ratner, Z. Best, B. Lee, A. Brooks, S. Xia, H. Wu, M.A. Kelliher, et al. 2018. Pathogen blockade of TAK1 triggers caspase-8-dependent cleavage of gasdermin D and cell death. *Science.* 362:1064–1069. https://doi.org/10.1126/science.aau2818

Orth, K., L.E. Palmer, Z.Q. Bao, S. Stewart, A.E. Rudolph, J.B. Bliska, and J.E. Dixon. 1999. Inhibition of the mitogen-activated protein kinase kinase superfamily by a *Yersinia* effector. *Science.* 285:1920–1923. https://doi.org/10.1126/science.285.5435.1920

Pelletier, S., S. Gingras, and D.R. Green. 2015. Mouse genome engineering via CRISPR-Cas9 for study of immune function. *Immunity.* 42:18–27. https://doi.org/10.1016/j.immuni.2015.01.004

Peterson, L.W., N.H. Philip, A. DeLaney, M.A. Wynosky-Dolfi, K. Asklof, F. Gray, R. Choa, E. Bjanes, E.L. Buza, B. Hu, et al. 2017. RIPK1-dependent apoptosis bypasses pathogen blockade of innate signaling to promote immune defense. *J. Exp. Med.* 214:3171–3182. https://doi.org/10.1084/jem.20170347

Poudel, B., and P. Gurung. 2018. An update on cell intrinsic negative regulators of the NLRP3 inflammasome. *J. Leukoc. Biol.* 103:1165–1177. https://doi.org/10.1002/JLB.3MIR0917-350R

Sanjo, H., J. Nakayama, T. Yoshizawa, H.J. Fehling, S. Akira, and S. Taki. 2019. Cutting edge: TAK1 safeguards macrophages against proinflammatory cell death. *J. Immunol.* 203:783–788. https://doi.org/10.4049/jimmunol.1900202

Sarhan, J., B.C. Liu, H.I. Muendlein, P. Li, R. Nilson, A.Y. Tang, A. Rongvaux, S.C. Bunnell, F. Shao, D.R. Green, and A. Poltorak. 2018. Caspase-8 induces cleavage of gasdermin D to elicit pyroptosis during *Yersinia* infection. *Proc. Natl. Acad. Sci. USA.* 115:E10888–E10897. https://doi.org/10.1073/pnas.1809548115

Shi, J., Y. Zhao, K. Wang, X. Shi, Y. Wang, H. Huang, Y. Zhuang, T. Cai, F. Wang, and F. Shao. 2015. Cleavage of GSDMD by inflammatory caspases determines pyroptotic cell death. *Nature.* 526:660–665. https://doi.org/10.1038/nature15514

Tenev, T., K. Bianchi, M. Darding, M. Broemer, C. Langlais, F. Wallberg, A. Zachariou, J. Lopez, M. MacFarlane, K. Cain, and P. Meier. 2011. The Ripoptosome, a signaling platform that assembles in response to genotoxic stress and loss of IAPs. *Mol. Cell.* 43:432–448. https://doi.org/10.1016/j.molcel.2011.06.006

Weinlich, R., and D.R. Green. 2014. The two faces of receptor interacting protein kinase-1. *Mol. Cell.* 56:469–480. https://doi.org/10.1016/j.molcel.2014.11.001

Xu, D., T. Jin, H. Zhu, H. Chen, D. Ofengeim, C. Zou, L. Mifflin, L. Pan, P. Amin, W. Li, et al. 2018. TBK1 suppresses RIPK1-driven apoptosis and inflammation during development and in aging. *Cell.* 174:1477–1491.e19. https://doi.org/10.1016/j.cell.2018.07.041

Zhang, H., X. Zhou, T. McQuade, J. Li, F.K. Chan, and J. Zhang. 2011. Functional complementation between FADD and RIP1 in embryos and lymphocytes. *Nature.* 471:373–376. https://doi.org/10.1038/nature09878

Supplemental material

Malireddi et al., https://doi.org/10.1084/jem.20191644

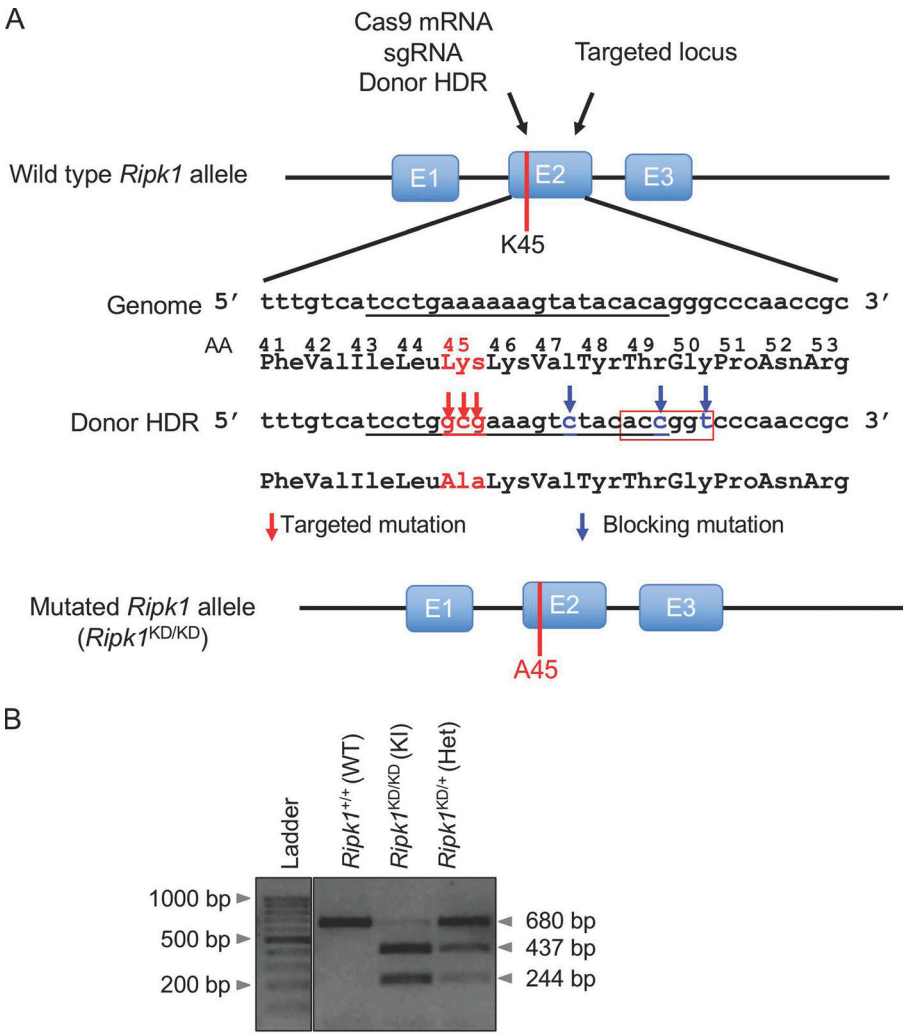

Figure S1. **Generation of *Ripk1*$^{KD/KD}$ mice using CRISPR/Cas9 technology. (A)** To generate the KD mutant allele, a donor homology-directed repair (HDR) was designed and used to substitute lysine (K) at amino acid (AA) position 45 of RIPK1 with alanine (A), as described in the Materials and methods section. The red arrows in the genomic sequence indicate the altered nucleotides designed for the substitution, and the blue arrows denote the blocking mutations that were introduced to prevent retargeting of the edited sequence by sgRNA. The red box indicates the silent substitutions that generate an AgeI restriction site and were inserted for genotyping purposes. **(B)** Genotyping of mutant and WT *Ripk1* allele using PCR amplification of tail DNA followed by restriction digestion using AgeI. Het, heterozygote; KI, knock-in.

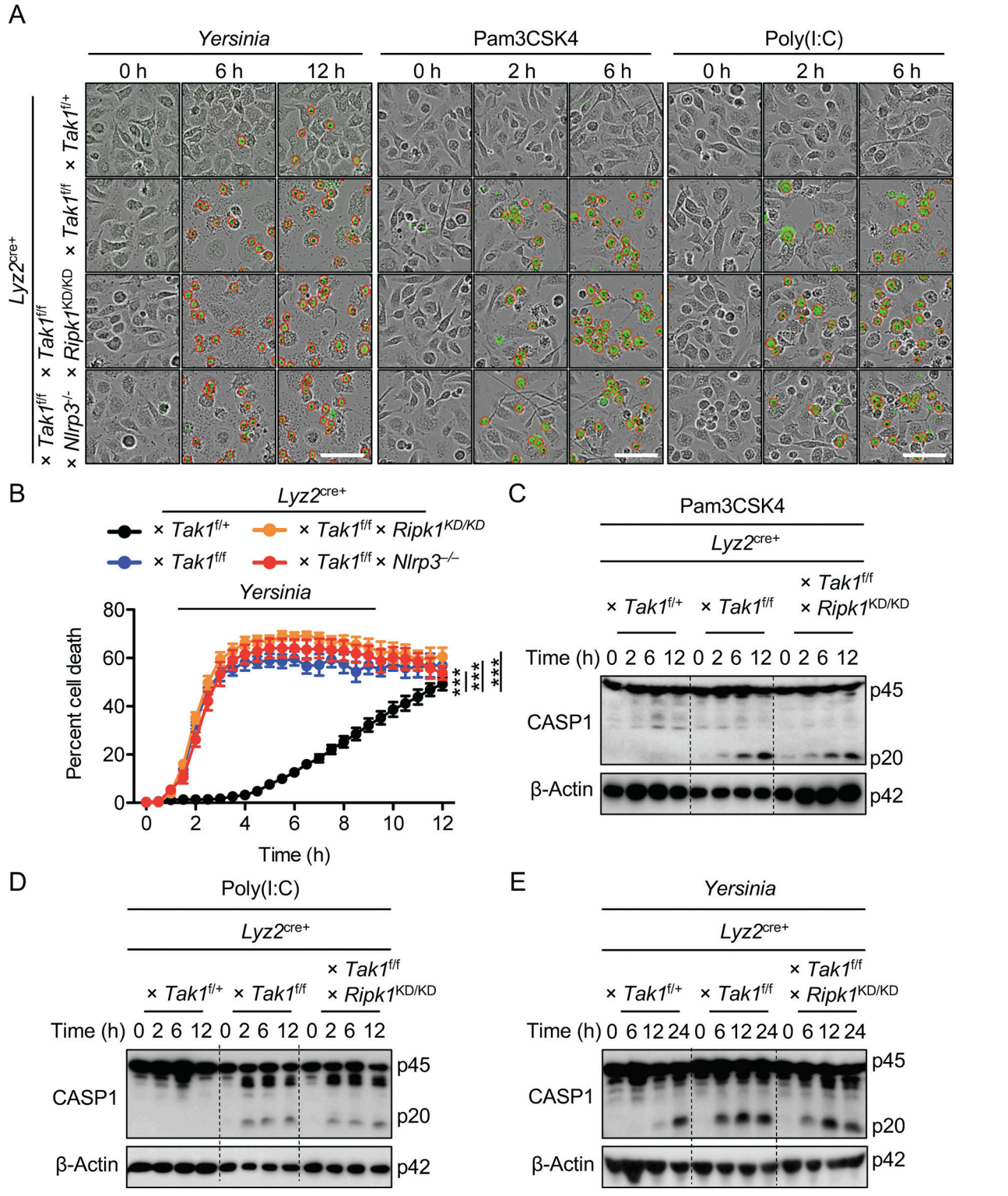

Figure S2. **Signaling through either TLR2 or TLR3 bypasses the requirement for RIPK1 kinase activity in promoting cell death and caspase-1 activation. (A)** Cell death detected by IncuCyte image analysis of BMDMs infected with *Y. enterocolitica* (MOI 5) or treated with TLR2 ligand Pam3CSK4 or TLR3 agonist poly(I:C). BMDMs were obtained from *Lyz2*$^{cre+}$ × *Tak1*$^{f/+}$, *Lyz2*$^{cre+}$ × *Tak1*$^{f/f}$, *Lyz2*$^{cre+}$ × *Tak1*$^{f/f}$ × *Ripk1*$^{KD/KD}$, and *Lyz2*$^{cre+}$ × *Tak1*$^{f/f}$ × *Nlrp3*$^{-/-}$ mice. Cell death of the BMDMs was assessed in culture at the indicated times after stimulation. Scale bars, 100 µm. **(B)** Time-course analysis of cell death in indicated BMDMs infected with *Y. enterocolitica* (MOI 5). P values < 0.05 were considered statistically significant. ***, P < 0.001 (one-way ANOVA with Dunnett's multiple comparisons test). **(C–E)** Western blot analysis of the active caspase-1 subunit p20 from the indicated BMDMs treated with Pam3CSK4 (C) or poly(I:C) (D) or BMDMs infected with *Y. enterocolitica* (E). The "p" in Western blots denotes protein molecular weight. Green with red circles indicates dead-cell positivity for the SYTOX Green stain. Data are presented as mean ± SEM (B) and are representative of five independent experiments with three (A and B) or two (C–E) technical replicates per sample.

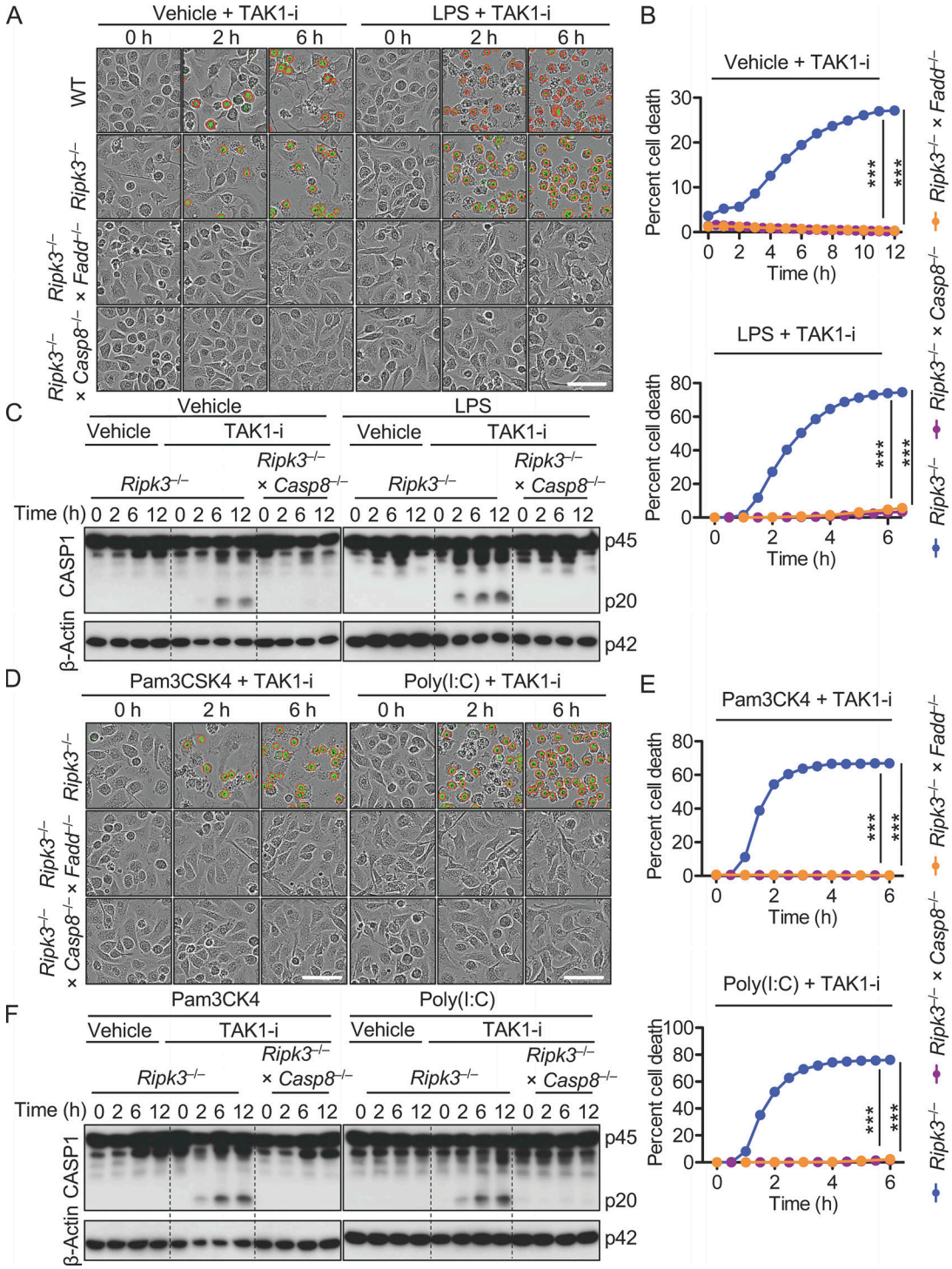

Figure S3. **During TAK1 inactivation, FADD and caspase-8 are required for cell death and inflammasome activation, both in the presence and in the absence of priming. (A)** Cell death detected by IncuCyte image analysis of BMDMs treated with vehicle or LPS in the presence of TAK1-i. BMDMs were obtained from WT, *Ripk3*$^{-/-}$, *Ripk3*$^{-/-}$ × *Fadd*$^{-/-}$, or *Ripk3*$^{-/-}$ × *Casp8*$^{-/-}$ mice. Scale bar, 100 µm. **(B)** Time-course analysis of cell death in BMDMs treated with vehicle or LPS in the presence of TAK1-i and assessed in culture at the indicated times. P values < 0.05 were considered statistically significant. ***, P < 0.001 (one-way ANOVA with Dunnett's multiple comparisons test). **(C)** Western blot analysis of the active caspase-1 subunit p20 in the BMDMs treated with vehicle or LPS in the presence of TAK1-i. BMDMs were assessed at 0, 2, 6, and 12 h in culture. **(D)** Cell death detected by IncuCyte image analysis of BMDMs treated with Pam3CSK4 or poly(I:C) in the presence of TAK1-i. Scale bars, 100 µm. **(E)** Time-course analysis of cell death of BMDMs treated with Pam3CSK4 or poly(I:C) in the presence of TAK1-i. P values < 0.05 were considered statistically significant. ***, P < 0.001 (one-way ANOVA with Dunnett's multiple comparisons test). **(F)** Western blot analysis of the active caspase-1 subunit p20 in the BMDMs treated with Pam3CSK4 or poly(I:C) in the presence or absence of TAK1-i. BMDMs were assessed at 0, 2, 6, and 12 h in culture. Green with red circles indicates dead-cell positivity for SYTOX Green stain. The "p" in Western blots denotes protein molecular weight. Data are representative of three independent experiments with three (A, B, D, and E) or two (C and F) technical replicates for each sample.

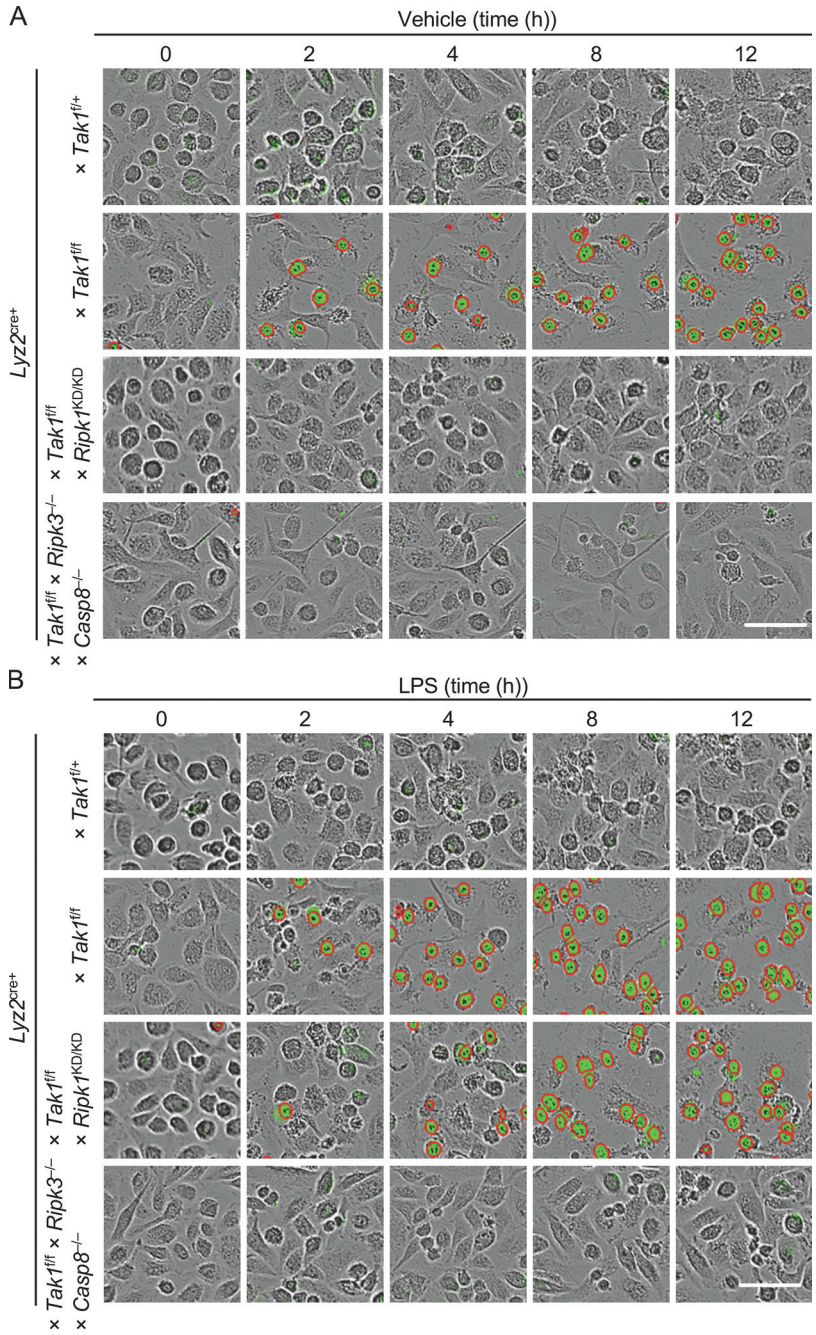

Figure S4. **Genetic deletion of RIPK3 and caspase-8 protects TAK1-deficient cells from cell death, both in the presence and in the absence of priming. (A and B)** Cell death detected by IncuCyte image analysis of BMDMs treated with vehicle control (A) or LPS (B) at indicated time points. BMDMs were obtained from *Lyz2*$^{cre+}$ × *Tak1*$^{f/+}$, *Lyz2*$^{cre+}$ × *Tak1*$^{f/f}$, *Lyz2*$^{cre+}$ × *Tak1*$^{f/f}$ × *Ripk1*$^{KD/KD}$, and *Lyz2*$^{cre+}$ × *Tak1*$^{f/f}$ × *Ripk3*$^{-/-}$ × *Casp8*$^{-/-}$ mice. Green with red circles indicates dead-cell positivity for the SYTOX Green stain. Scale bars, 50 µm. Data are representative of three independent experiments with four technical replicates for each sample (A and B).

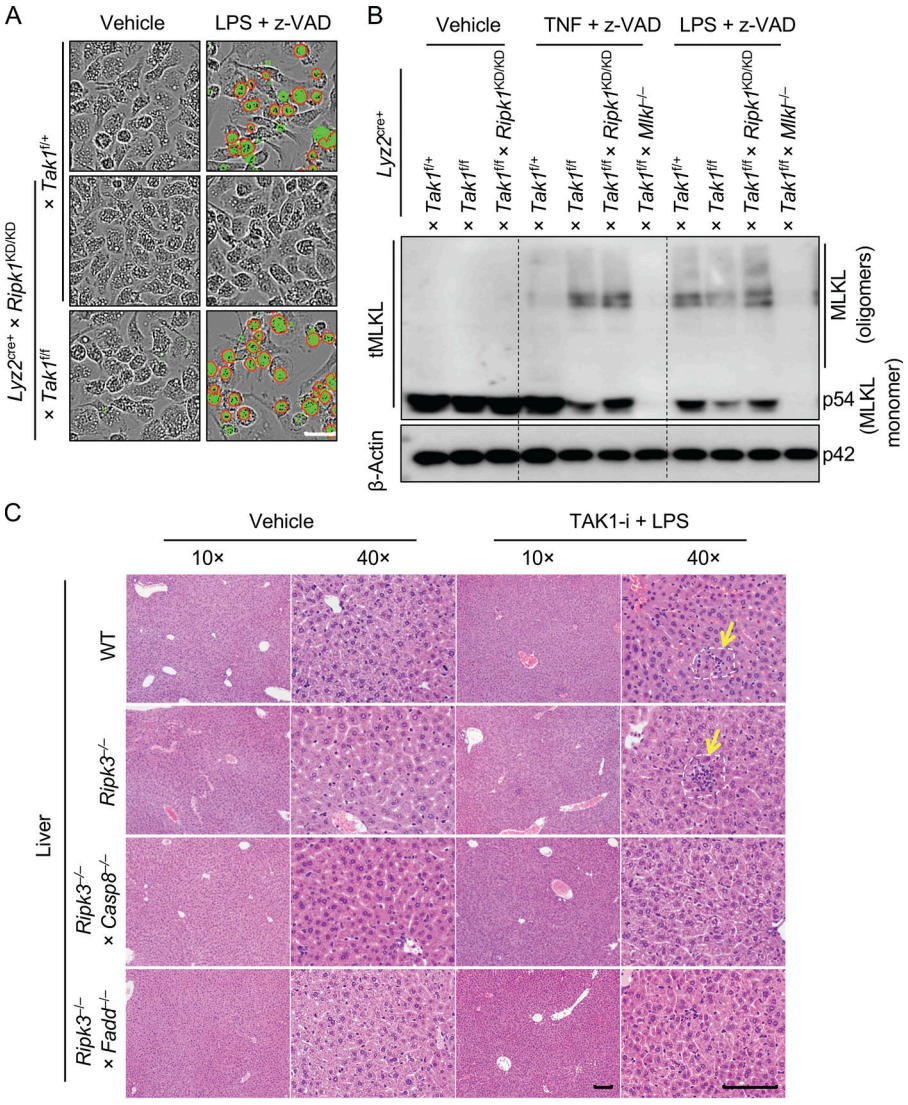

Figure S5. **Genetic deletion of caspase-8 rescues TAK1 inactivation–induced inflammatory cell death of myeloid cells, and FADD deletion rescues TAK1-deficient mice from the pathophysiology of sepsis. (A)** Cell death detected by IncuCyte image analysis of BMDMs treated with vehicle or LPS + z-VAD. BMDMs were obtained from *Lyz2*$^{cre+}$ × *Tak1*$^{f/+}$, *Lyz2*$^{cre+}$ × *Tak1*$^{f/+}$ × *Ripk1*$^{KD/KD}$, and *Lyz2*$^{cre+}$ × *Tak1*$^{f/f}$ × *Ripk1*$^{KD/KD}$ mice and assessed in culture at 12 h after stimulation. Green with red circles indicates dead-cell positivity for the SYTOX Green stain. Scale bar, 50 µm. **(B)** Western blot analysis of MLKL protein expression and oligomerization from BMDMs prepared from *Lyz2*$^{cre+}$ × *Tak1*$^{f/+}$, *Lyz2*$^{cre+}$ × *Tak1*$^{f/f}$, *Lyz2*$^{cre+}$ × *Tak1*$^{f/f}$ × *Ripk1*$^{KD/KD}$, and *Lyz2*$^{cre+}$ × *Tak1*$^{f/f}$ × *Mlkl*$^{-/-}$ mouse strains that were treated with vehicle control, TNF + z-VAD, or LPS + z-VAD. **(C)** Histopathologic analysis by hematoxylin and eosin–stained sections of livers from WT littermate controls, *Ripk3*$^{-/-}$, *Ripk3*$^{-/-}$ × *Casp8*$^{-/-}$, and *Ripk3*$^{-/-}$ × *Fadd*$^{-/-}$ mice 6 h after LPS + TAK1-i–induced septic shock. Yellow arrows indicate focal granulocytic infiltration. Scale bars, 50 µm. *n* = 3. Data are representative of three (A) or two (B and C) independent experiments.